The Astronomical Journal, 132:1669–1691, 2006 October

WIDE-FIELD CCD PHOTOMETRY AROUND NINE OPEN CLUSTERS

Saurabh Sharma,[1] A. K. Pandey,[1] K. Ogura,[2] H. Mito,[3] K. Tarusawa,[3] and R. Sagar[1]

Received 2006 February 2; accepted 2006 June 20

ABSTRACT

In this paper we study the evolution of the core and corona of nine open clusters using the projected radial density profiles derived from homogeneous CCD photometric data obtained with the 105 cm Kiso Schmidt telescope. The age and galactocentric distance of the target clusters vary from 16 to 2000 Myr and 9 to 10.8 kpc, respectively. Barring Be 62, which is a young open cluster, other clusters show a uniform reddening across the cluster region. The reddening in Be 62 varies from $E(B-V)_{\rm min} = 0.70$ mag to $E(B-V)_{\rm max} = 1.00$ mag. The coronae of six of the clusters in the present sample are found to be elongated; however, on the basis of the present sample it is not possible to establish any correlation between the age and shape of the core. The elongated core in the case of the young cluster Be 62 may reflect the initial conditions in the parental molecular cloud. The other results of the present study are as follows: (1) Core radius r_c and corona size $r_{\rm cn}$/cluster radius $r_{\rm cl}$ are linearly correlated. (2) The r_c, $r_{\rm cn}$, and $r_{\rm cl}$ are linearly correlated with the number of stars in that region. (3) In the age range 10–1000 Myr, the core and corona shrink with age. (4) We find that in the galactocentric distance range 9–10 kpc, the core and corona/cluster extent of the clusters increase with the galactocentric distance.

Key words: open clusters and associations: general — techniques: photometric

Online material: machine-readable table

1. INTRODUCTION

The study of Galactic open clusters is of great interest in several astrophysical aspects. Young open clusters provide information about current star formation processes and are key objects for clarifying questions of Galactic structure, while observations of old and intermediate-age open clusters play an important role in studying the theories of stellar and Galactic evolution.

The nucleus and the corona (extended region of the star cluster) are the two main regions in open clusters (Kholopov 1969). The nucleus of a cluster contains relatively bright and massive ($\geq 3\ M_\odot$) stars, whereas the corona, which contains a large number of faint and low-mass ($\leq 1\ M_\odot$) stars, has an important bearing on studies related to the mass function (MF), the structure, and the evolution of open clusters. A detailed analysis of the structure of coronae of open clusters is needed to understand the effects of external environments, like the Galactic tidal field and impulsive encounters with interstellar clouds, etc., on dynamical evolution of open clusters (Pandey et al. 1990). Extensive studies of the coronal regions of clusters have not been carried out so far mainly because of unavailability of photometry in a large field around open star clusters.

A $2\mathrm{K} \times 2\mathrm{K}$ CCD mounted on a Schmidt telescope (Kiso, Japan), covering a $\sim 50' \times 50'$ field, can be used to get photometry in a large field around open star clusters. The ability to obtain improved photometry of thousands of stars means that large-scale studies of open clusters can be conducted to study the spatial structure and stability of Galactic open clusters. With the addition of photometry of a nearby field region it is possible to construct luminosity functions (LFs) and MFs, which are useful for understanding cluster-formation processes and the theory of star formation in open clusters (Miller & Scalo 1979).

Considering the importance of low-mass stars in the coronae of star clusters, we have generated a wide-field photometric database around nine open star clusters with the aim of reinvestigating the clusters' parameters, e.g., reddening, distance, age, their size, and their LF/MF, using a homogeneous database. The basic parameters of the clusters, taken from WEBDA[4] (Mermilliod 1995), are given in Table 1.

2. OBSERVATIONS AND DATA REDUCTIONS

The broadband CCD photometric observations of clusters were carried out from 2001 November 19 to 25 using the 105 cm Schmidt telescope of the Kiso Observatory. The CCD camera used a SITe 2048×2048 pixel^2 TK2048E chip having a pixel size of 24 μm. At the Schmidt focus (f/3.1), each pixel of the CCD corresponds to $1\farcs5$, and the entire chip covers a field of $\sim 50' \times 50'$ on the sky. The readout noise and gain of the CCD are 23.2 and 3.4 e^- ADU^{-1}, respectively.

The observations of NGC 1528, NGC 2287, NGC 2301, NGC 2323, NGC 2420, NGC 2437, and NGC 2548 were standardized by observing standard stars in SA 95 (Landolt 1992) with brightness $12.2 < V < 15.6$ and color $0.45 < (B-V) < 1.51$ on four nights from 2001 November 22 to 25. To standardize the observation of Be 62 and NGC 1960 we generated a secondary standard in the field of these two clusters by observing stars in SA 95 on 2001 November 24 and 22, respectively. A number of bias and dome-flat frames were also taken during the observing runs. The log of observations is given in Table 2. A number of short and deep exposure frames have been obtained for all the clusters.

The CCD data frames were reduced using computing facilities available at the Aryabhatta Research Institute of Observational Sciences (ARIES), Nainital. Initial processing of the data frames was done using the IRAF[5] and ESO-MIDAS[6] data reduction

[1] Aryabhatta Research Institute of Observational Sciences, Manora Peak, Nainital 263 129, India.
[2] Kokugakuin University, Higashi, Shibuya-ku, Tokyo 150-8440, Japan.
[3] Kiso Observatory, School of Science, University of Tokyo, Mitake-mura, Kiso-gun, Nagano 397-0101, Japan.

[4] See http://obswww.unige.ch/webda.
[5] IRAF is distributed by the National Optical Astronomy Observatory.
[6] ESO-MIDAS is developed and maintained by the European Southern Observatory.

TABLE 1
CLUSTER PARAMETERS FROM WEBDA

Cluster	Cluster No. (IAU)	Trumpler Class	$\alpha_{2000.0}$	$\delta_{2000.0}$	l (deg)	b (deg)	Log Age (yr)	Distance (pc)	$E(B-V)$ (mag)
Be 62.....	C0057+636	III2m	01 01 00	+63 57 00	123.98	1.10	7.2	1837	0.85
NGC 1528.....	C0411+511	II2m	04 15 23	+51 12 54	152.06	0.26	8.6	776	0.26
NGC 1960.....	C0532+341	I3r	05 36 18	+34 08 24	174.52	1.07	7.5	1318	0.22
NGC 2287.....	C0644−206	I3r	06 46 01	−20 45 24	231.02	−10.44	8.4	693	0.03
NGC 2301.....	C0649+005	I3r	06 51 45	+00 27 36	212.56	0.28	8.2	872	0.03
NGC 2323.....	C0700−082	II3r	07 02 42	−08 23 00	221.67	−1.33	8.1	929	0.21
NGC 2420.....	C0735+216	I1r	07 38 23	+21 34 24	198.11	19.63	9.1	3085	0.03
NGC 2437.....	C0739−147	II2r	07 41 46	−14 48 36	231.86	4.06	8.4	1375	0.15
NGC 2548.....	C0811−056	I3r	08 13 43	−05 45 00	227.87	15.39	8.6	769	0.03

NOTE.—Units of right ascension are hours, minutes, and seconds, and units of declination are degrees, arcminutes, and arcseconds.

packages. Photometry of cleaned frames was carried out using DAOPHOT-II software (Stetson 1987). The point-spread function (PSF) was obtained for each frame using several uncontaminated stars. The FWHM of the star images varied between 3″ and 4″ from night to night. When brighter stars were saturated on deep-exposure frames their magnitudes were taken from short-exposure frames. We used the DAOGROW program for the construction of an aperture growth curve required for determining the difference between aperture and profile-fitting magnitudes. Calibration of the instrumental magnitude to the standard system

TABLE 2
LOG OF OBSERVATIONS

Field	Filter	Exposure (in Seconds) × No. of Frames	Date
Be 62.....	U	$180\times11,\ 60\times3$	2001 Nov 20
	B	$90\times9,\ 30\times2,\ 20\times5$	2001 Nov 20
	V	$90\times9,\ 20\times6$	2001 Nov 20
	R	$60\times12,\ 10\times8$	2001 Nov 21
	I	$60\times9,\ 20\times1,\ 10\times6$	2001 Nov 21
NGC 1528.....	B	$60\times7,\ 10\times7$	2001 Nov 23
	V	$60\times7,\ 10\times7$	2001 Nov 23
	R	$60\times7,\ 10\times7,\ 5\times9$	2001 Nov 23
	I	$60\times7,\ 10\times7,\ 5\times9$	2001 Nov 23
NGC 1960.....	U	$180\times8,\ 30\times6$	2001 Nov 21
	B	$60\times6,\ 20\times6,\ 10\times3$	2001 Nov 21
	V	$60\times6,\ 30\times3,\ 10\times2$	2001 Nov 21
	R	$30\times9,\ 10\times6$	2001 Nov 21
	I	$30\times9,\ 10\times6,\ 5\times2$	2001 Nov 21
NGC 2287.....	B	$60\times4,\ 10\times4,\ 5\times3$	2001 Nov 25
	V	$60\times4,\ 10\times4,\ 5\times3$	2001 Nov 25
	I	$60\times1,\ 30\times3,\ 10\times4,\ 5\times5$	2001 Nov 25
NGC 2301.....	U	$180\times8,\ 60\times8$	2001 Nov 22
	B	$60\times8,\ 20\times1,\ 10\times7$	2001 Nov 22
	V	$60\times9,\ 10\times7$	2001 Nov 22
	I	$60\times8,\ 10\times7$	2001 Nov 22
NGC 2323.....	U	$180\times9,\ 60\times9$	2001 Nov 19
	U	180×3	2001 Nov 24
	B	$60\times4,\ 10\times12$	2001 Nov 19
	B	60×2	2001 Nov 24
	V	$60\times3,\ 10\times9$	2001 Nov 20
	V	60×2	2001 Nov 24
	I	$30\times6,\ 10\times9$	2001 Nov 20
	I	10×1	2001 Nov 24
NGC 2420.....	B	$60\times2,\ 10\times1$	2001 Nov 24
	V	$60\times9,\ 20\times6,\ 10\times3$	2001 Nov 24
	I	$60\times9,\ 10\times9$	2001 Nov 24
NGC 2437.....	B	$60\times9,\ 20\times6$	2001 Nov 24
	B	$60\times1,\ 20\times1$	2001 Nov 25
	V	$60\times9,\ 20\times6,\ 10\times3$	2001 Nov 24
	V	$60\times1,\ 20\times1$	2001 Nov 25
	I	$60\times6,\ 30\times3,\ 10\times3$	2001 Nov 25
NGC 2548.....	V	$60\times6,\ 10\times6$	2001 Nov 25
	I	$60\times4,\ 10\times4,\ 5\times2$	2001 Nov 25

TABLE 3

THE ZERO-POINT CONSTANTS, COLOR COEFFICIENTS, AND EXTINCTION COEFFICIENTS ON DIFFERENT NIGHTS

PARAMETERS	DATE			
	2001 Nov 22	2001 Nov 23	2001 Nov 24	2001 Nov 25
Zero-point constant:				
c_1	6.305 ± 0.005	...	6.189 ± 0.011	...
c_2	2.553 ± 0.005	2.562 ± 0.003	2.488 ± 0.003	2.920 ± 0.006
c_3	2.882 ± 0.005	2.893 ± 0.004	2.841 ± 0.004	3.198 ± 0.008
c_4	2.564 ± 0.006	2.567 ± 0.004	2.531 ± 0.005	...
c_5	3.545 ± 0.007	3.532 ± 0.007	3.491 ± 0.005	3.762 ± 0.010
Color coefficient:				
m_1	-0.045 ± 0.008	...	-0.014 ± 0.010	...
m_2	-0.116 ± 0.004	-0.125 ± 0.003	-0.112 ± 0.003	-0.136 ± 0.006
m_3	0.068 ± 0.005	0.068 ± 0.004	0.070 ± 0.003	0.067 ± 0.006
m_4	0.031 ± 0.009	0.040 ± 0.007	0.047 ± 0.007	...
m_5	-0.076 ± 0.006	-0.076 ± 0.006	-0.061 ± 0.004	-0.083 ± 0.008
Extinction coefficient:				
k_u	0.661 ± 0.028	...	0.683 ± 0.028	...
k_b	0.261 ± 0.012	0.352 ± 0.007	0.295 ± 0.007	0.211 ± 0.012
k_v	0.176 ± 0.010	0.218 ± 0.012	0.183 ± 0.008	0.133 ± 0.015
k_r	0.150 ± 0.009	0.181 ± 0.012	0.128 ± 0.010	...
k_i	0.047 ± 0.009	0.140 ± 0.021	0.096 ± 0.010	0.037 ± 0.020

was done using the procedure outlined by Stetson (1992). The photometric calibration equations used were

$$u = U + c_1 + m_1(U - B) + k_u X,$$

$$b = B + c_2 + m_2(B - V) + k_b X,$$

$$v = V + c_3 + m_3(V - I) + k_v X,$$

$$r = R + c_4 + m_4(V - R) + k_r X,$$

$$i = I + c_5 + m_5(V - I) + k_i X,$$

where U, B, V, R, and I are the standard magnitudes; u, b, v, r, and i are the instrumental magnitudes normalized for 1 s of exposure time; X is the air mass; c_1, c_2, c_3, c_4, and c_5 and m_1, m_2, m_3, m_4, and m_5 are zero-point constants and color coefficients, respectively; and k_u, k_b, k_v, k_r, and k_i are extinction coefficients in the U, B, V, R and I bands, respectively. The values of the zero-point constants, color coefficients, and extinction coefficients in various bands on different nights are given in Table 3. Figure 1 shows the standardization residual, Δ, between standard and transformed V magnitude and $(U - B)$, $(B - V)$, $(V - R)$, and $(V - I)$ colors of standard stars. The standard deviations in ΔV, $\Delta(U - B)$, $\Delta(B - V)$, $\Delta(V - R)$, and $\Delta(V - I)$ are 0.017, 0.060, 0.028, 0.023, and 0.020 mag respectively. The typical DAOPHOT errors in magnitude and colors along with parameter χ and sharpness as a function of V magnitude in the case of clusters Be 62 and NGC 1960 are shown in Figure 2. It can be seen that the errors become

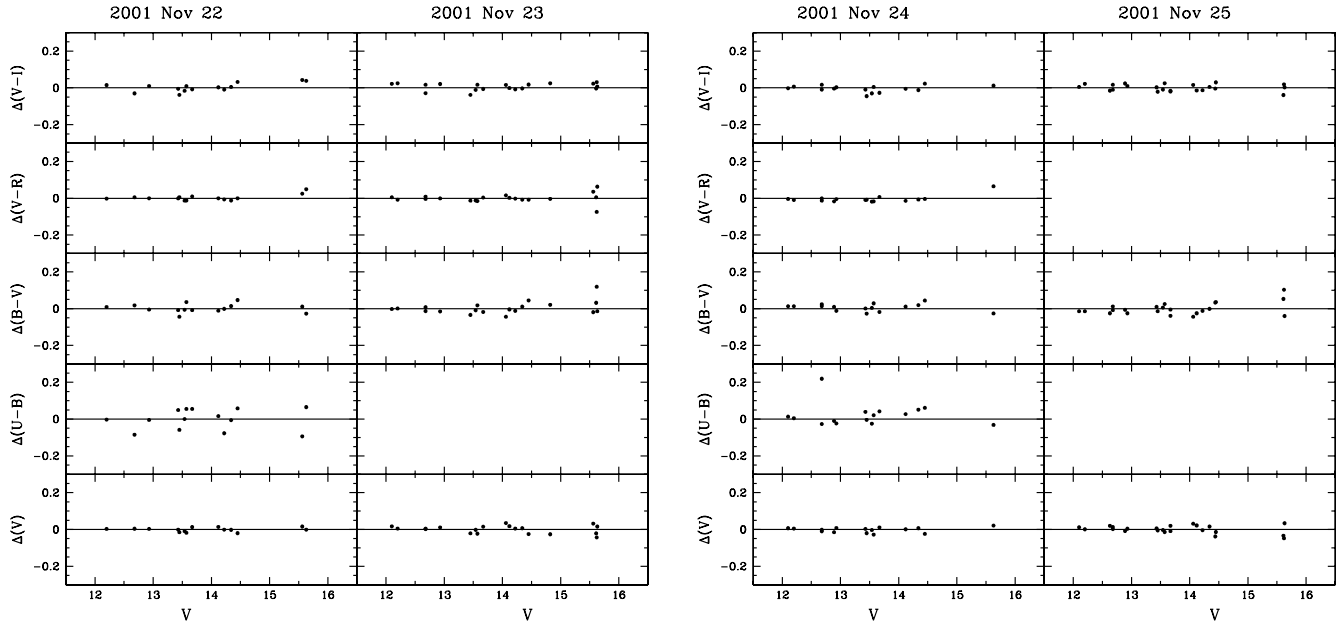

FIG. 1.—Residuals between standard and transformed magnitudes and colors of standard stars plotted against standard magnitude.

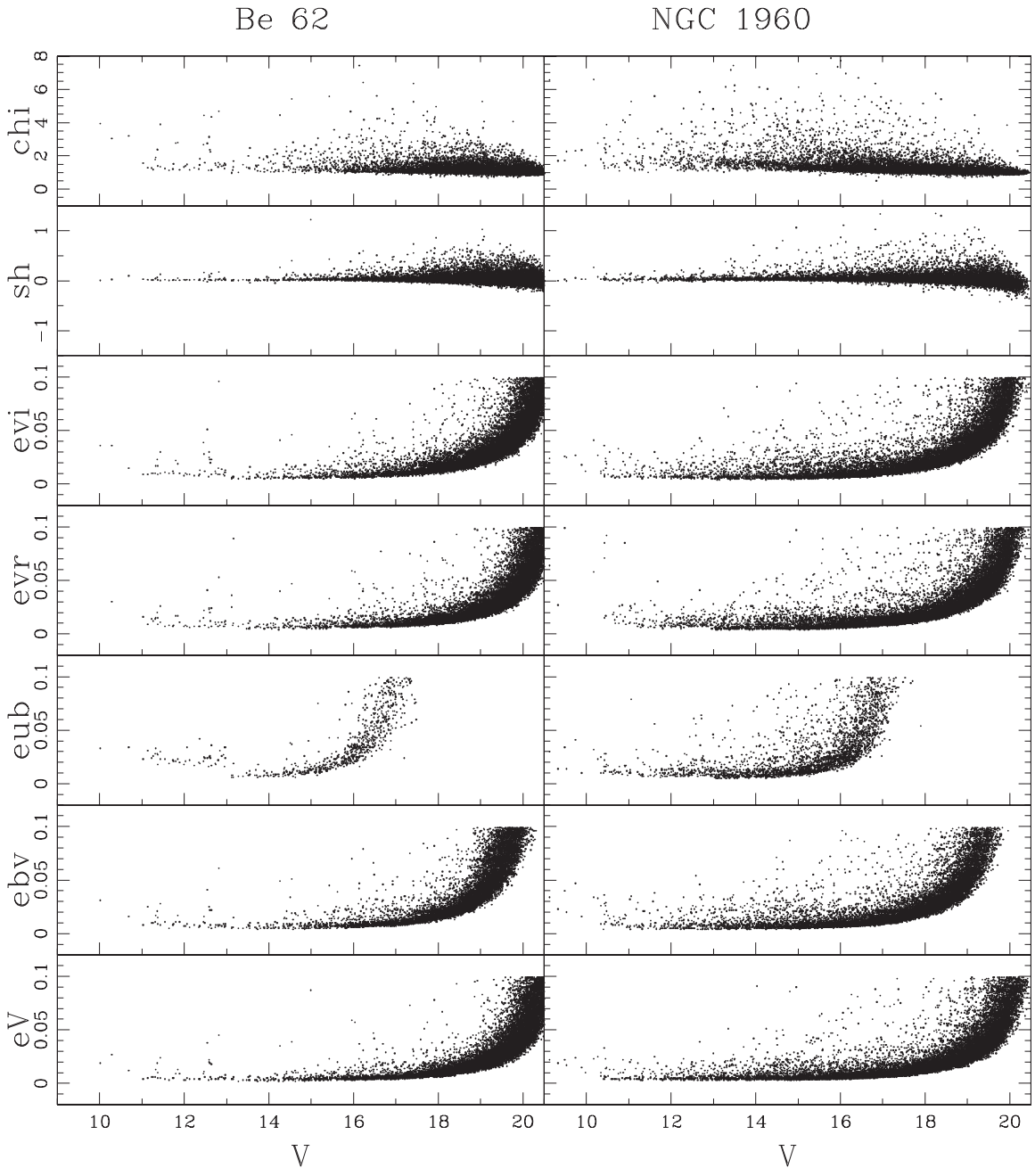

FIG. 2.—DAOPHOT errors, image parameter χ, and sharpness as a function of V magnitude for the measurements of Be 62 and NGC 1960.

larger ($\geq$0.1 mag) for stars fainter than $V = 20$ mag; therefore, measurements below this magnitude are not reliable.

3. COMPARISON WITH PREVIOUS STUDIES

We have carried out a comparison of the present data with those available in the literature. The difference Δ (literature minus present data) as a function of V magnitude is shown in Figure 3, and the statistical results are given in Table 4. The comparison indicates rather a large scatter in Δ for photographic data as compared to the Δ-values for CCD photometry. Comparison of the photometry in the case of each cluster is discussed below.

Be 62.—CCD V magnitude and $(B - V)$ colors obtained by Phelps & Janes (1994) are in good agreement with those obtained in the present work. However, the photoelectric V magnitudes in the range 13–14 obtained by Forbes (1981) are brighter by $\sim$0.13 mag than that obtained in the present work. The $(U - B)$ colors obtained in the present work for stars having $V \sim 13$–16 mag are redder than those reported by Phelps & Janes (1994). For stars with $V > 17$ mag, the $(U - B)$ colors obtained by Phelps & Janes (1994) show a strong variation with V magnitude and become redder by $\sim$1.2 mag at $V \sim 18$–19 mag. Our $(U - B)$ colors for stars with $V = 13$–14 mag are in agreement with the photoelectric observations by Forbes (1981).

NGC 1528.—The V magnitude and $(B - V)$ colors obtained in the present work are in agreement with those reported by Hoag et al. (1961, hereafter H61).

NGC 1960.—The comparison of the present CCD photometry with the available photoelectric (Johnson & Morgan 1953) and photographic (Barkhatova et al. 1984, p. 118) photometry indicates a fair agreement between the different measurements. The

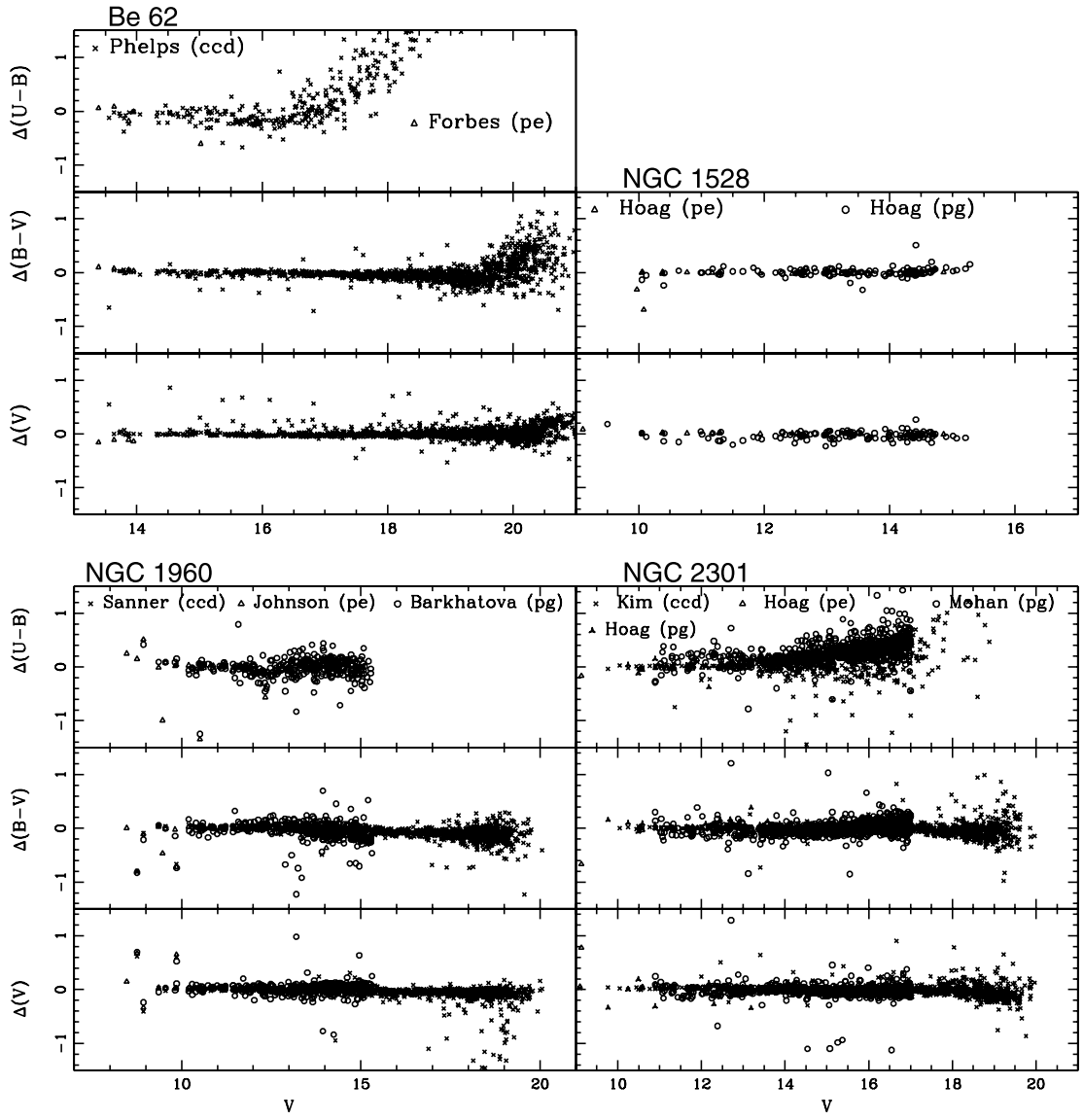

FIG. 3.—Comparison of the present CCD photometry with the data available in the literature. The difference Δ (literature minus present data) as a function of V magnitude for all the target clusters is shown. In the figure, pe, pg, and ccd indicate photoelectric, photographic, and CCD photometry, respectively.

V magnitude and $(B - V)$ colors obtained by us for stars with $V \leq 15$ mag are in good agreement with those given by Sanner et al. (2000; CCD photometry), whereas the V magnitudes obtained by us for stars fainter than $V = 15$ mag are systematically fainter by $\sim$0.06 mag, and the $(B - V)$ color shows a trend with increasing V magnitude in the sense that colors obtained by us become redder.

NGC 2287.—Photoelectric V magnitudes by Eggen (1974) are in agreement with the present observations, whereas photoelectric V magnitudes given by Harris et al. (1993), Ianna et al. (1987), and H61 are systematically fainter by $\sim$0.05 mag. The $(B - V)$ colors obtained in the present work are in agreement with those reported by Harris et al. (1993), Eggen (1974), and Ianna et al. (1987). The $(B - V)$ colors obtained by H61 are systematically bluer by $\sim$0.06 mag than the $(B - V)$ colors reported in the present work.

NGC 2301.—The V magnitude and $(B - V)$ colors obtained in the present work are in agreement with those reported in the literature. The $(U - B)$ colors for stars with $V \leq 16$ mag by Kim et al. (2001) are in agreement with the present results, whereas stars with $V > 16$ mag show a trend in $(U - B)$ color in the sense that the present colors become bluer with increasing V magnitude. The $(U - B)$ photographic colors reported by Mohan & Sagar (1988) at $V \sim 10$–13 mag are systematically redder by $\sim$0.12 mag and become redder with increasing V magnitude, whereas the photographic $(U - B)$ colors for stars with $V = 13$–15 mag by H61 are systematically redder by $\sim$0.12 mag.

NGC 2323.—The comparison indicates that the V magnitudes obtained by us are in general in agreement with those given in the literature, barring the magnitudes given by H61. The V magnitudes reported by H61 are fainter by $\sim$0.06 mag. The $(B - V)$ colors also show a fair agreement with the values reported in the literature excepting $(B - V)$ colors for $V \geq 13.0$ mag given by H61, which are bluer by $\sim$0.07 mag. The $(U - B)$ colors given in the literature also show a fair agreement with those obtained in the present study.

NGC 2420.—The comparison of the present CCD observations indicates a good agreement with those reported in the literature.

NGC 2437.—The comparison of the present CCD photometry with the available photographic, photoelectric, and CCD photometry indicates a good agreement between various reported observations.

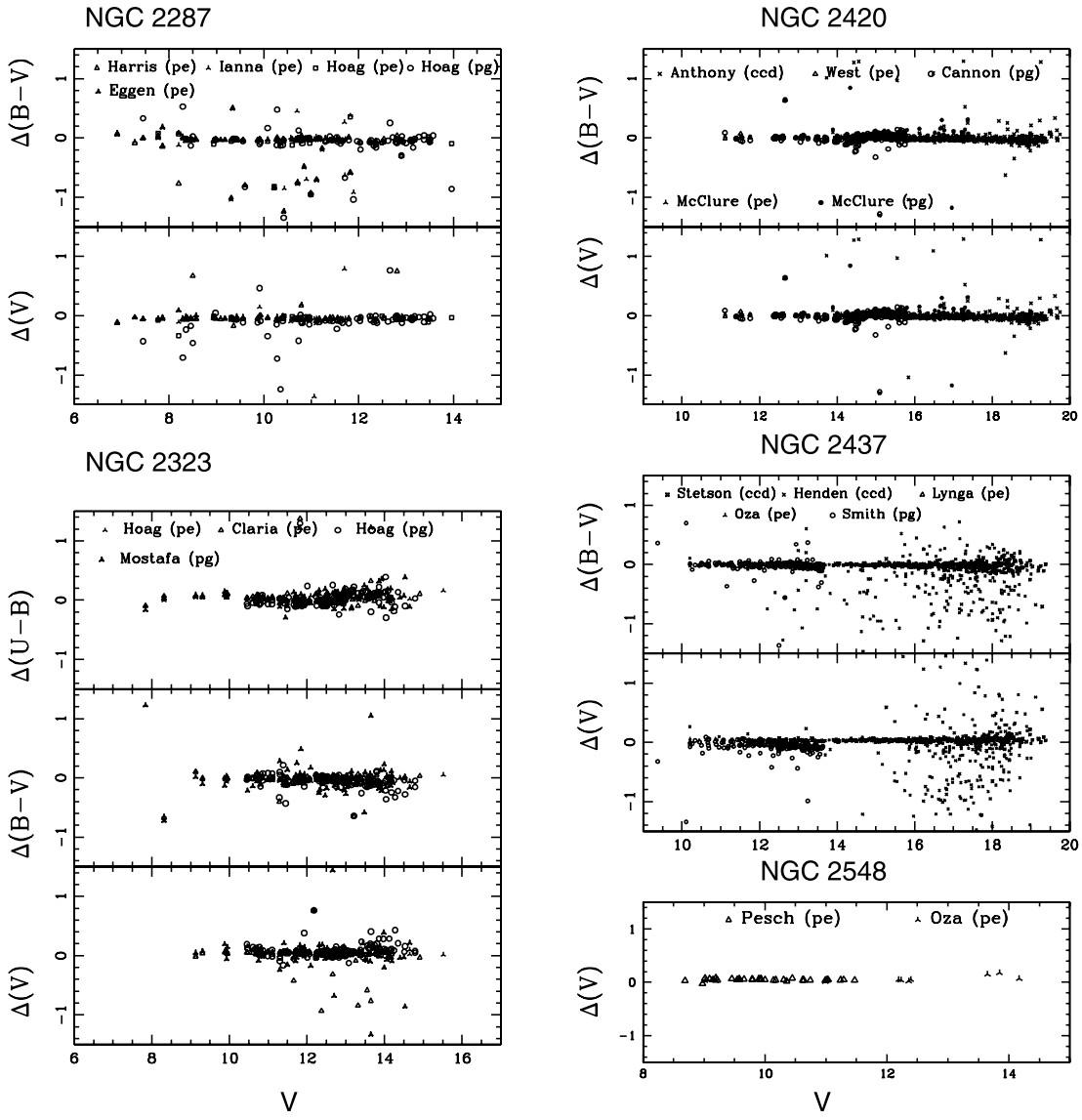

FIG. 3.—*Continued*

TABLE 4

COMPARISON OF THE PRESENT PHOTOMETRY WITH THE AVAILABLE PHOTOMETRY IN THE LITERATURE

Cluster Name	Reference	V Range	$\Delta(V)$ (Mean $\pm$ σ)	N	$\Delta(B-V)$ (Mean $\pm$ σ)	N	$\Delta(U-B)$ (Mean $\pm$ σ)	N
Be 62.....	Phelps & Janes (1994; ccd)	13–14	0.010 ± 0.033	9	0.022 ± 0.023	9	-0.112 ± 0.123	9
		14–15	0.021 ± 0.066	30	-0.021 ± 0.068	30	-0.073 ± 0.106	27
		15–16	0.002 ± 0.053	65	-0.005 ± 0.057	65	-0.129 ± 0.126	57
		16–17	-0.002 ± 0.063	92	-0.017 ± 0.052	92	-0.023 ± 0.223	74
		17–18	-0.002 ± 0.057	165	-0.045 ± 0.060	165	0.394 ± 0.321	64
		18–19	0.007 ± 0.070	239	-0.064 ± 0.087	239	1.227 ± 0.420	30
		19–20	0.010 ± 0.089	328	-0.022 ± 0.193	315	1.480 ± 0.000	1
		20–21	0.043 ± 0.149	285	0.267 ± 0.318	199	...	...
Be 62.....	Forbes (1981; pe)	13–14	-0.129 ± 0.024	4	0.062 ± 0.030	4	-0.014 ± 0.122	4
NGC 1528.....	Hoag et al. (1961; pe)	<11	0.024 ± 0.031	6	0.001 ± 0.014	5	...	...
		11–12	0.011 ± 0.008	4	-0.006 ± 0.006	4	...	...
		12–13	-0.001 ± 0.015	5	-0.006 ± 0.008	5	...	...

NOTES.—The difference Δ (literature minus present data) is in magnitudes. Mean and σ are based on N stars in a V-magnitude bin. Table 4 is published in its entirety in the electronic edition of the *Astronomical Journal*. A portion is shown here for guidance regarding its form and content.

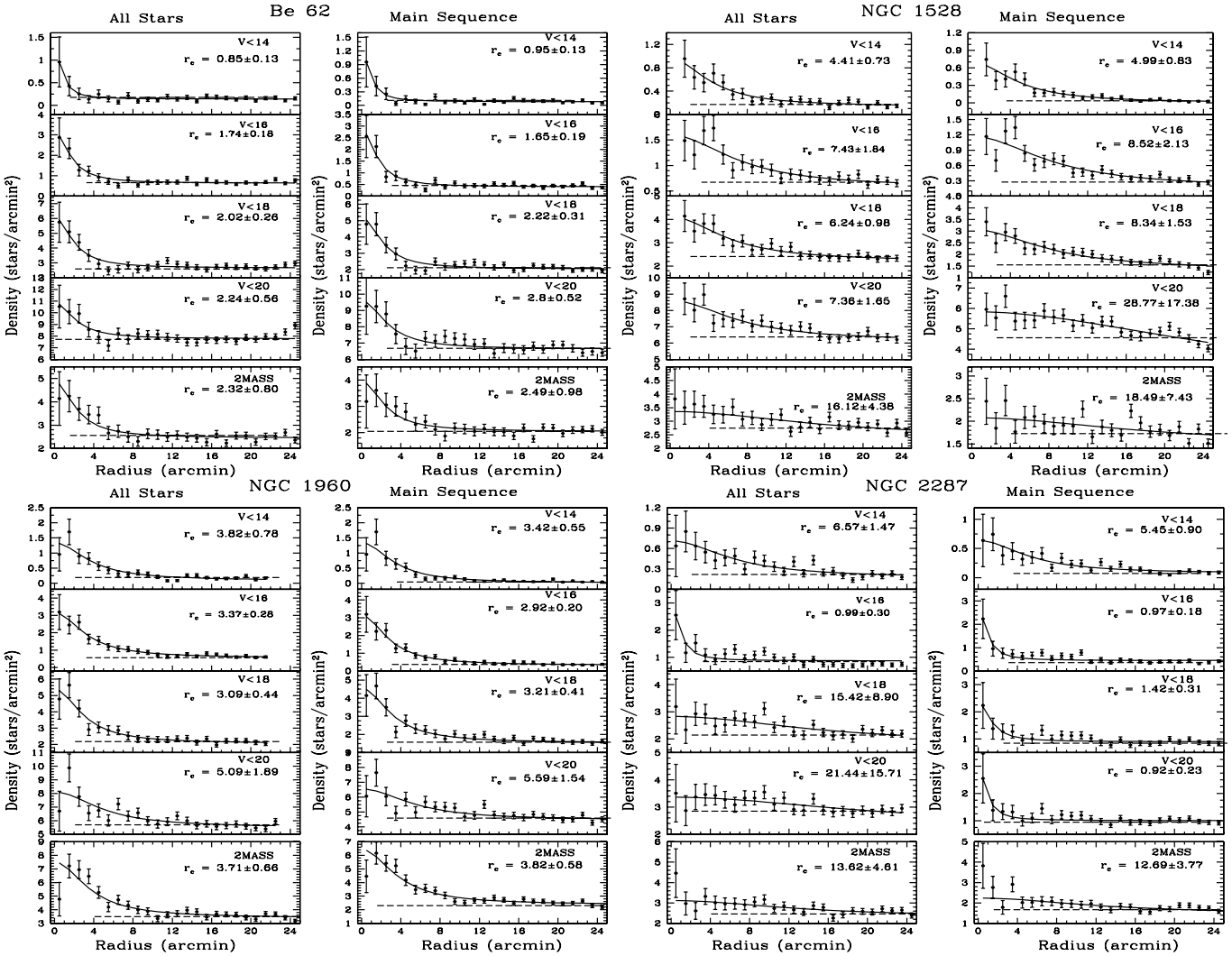

FIG. 4.—Radial density profiles of clusters Be 62, NGC 1528, NGC 1960, NGC 2287, NGC 2301, NGC 2323, NGC 2420, NGC 2437, and NGC 2548 for different magnitude levels using the present optical and 2MASS data. The solid curve shows a least-squares fit of the King (1962) profile to the observed data points (see text). The error bars represent $1/\sqrt{N}$ errors. The dashed line indicates the density of field stars.

NGC 2548.—The photoelectric V magnitudes by Pesch (1961) and Oja[7] are systematically fainter by about 0.05 mag.

4. ANALYSIS

4.1. *Radial Stellar Surface Density and Cluster Radius*

As the area of present CCD observations is quite large, it can be used to study the radial extent, structure (core and corona region), and evolutionary aspects of clusters. Since the projected distribution of stars in a cluster follows a systematic distribution from the center to the outer region, the center of the cluster was estimated by convolving a Gaussian kernel with the stellar distribution and taking the point of maximum density as the center. This was performed for both axes to get the center coordinates of the clusters. To determine the radial surface density the cluster was divided into a number of concentric rings. The projected radial stellar density in each concentric circle was obtained by dividing the number of stars in each annulus by its area, and the same is plotted in Figure 4 for various magnitude levels. The error bars are derived assuming that the number of stars in each annulus follows Poisson statistics. The extent of the cluster $r_{\rm cl}$ is defined as the point at which the radial density becomes constant. The horizontal dashed line in the plots indicates the density of contaminating field stars, which is obtained from the region outside (about 1.5 cluster radii) the cluster area.

To check whether the density distributions shown in Figure 4 (*left panels*) are affected by contamination due to field stars, we selected a sample of stars near a well-defined main sequence (MS) in the color-magnitude diagram (CMD), as mentioned by Pandey et al. (2001). The radial density distribution of the MS sample is shown in Figure 4 (*right panels*). Both samples in general show almost similar radial density profiles.

The observed radial density profile of the clusters was parameterized following the approach by Kaluzny & Udalski (1992) in which the projected radial density $\rho(r)$ is described as

$$\rho(r) \propto \frac{f_0}{1 + (r/r_c)^2},$$

where the cluster's core radius r_c is the radial distance at which the value of $\rho(r)$ becomes half of the central density f_0. The best

[7] See http://www.univie.ac.at/webda/cgi-bin/frame_detail.cgi?ngc2548.

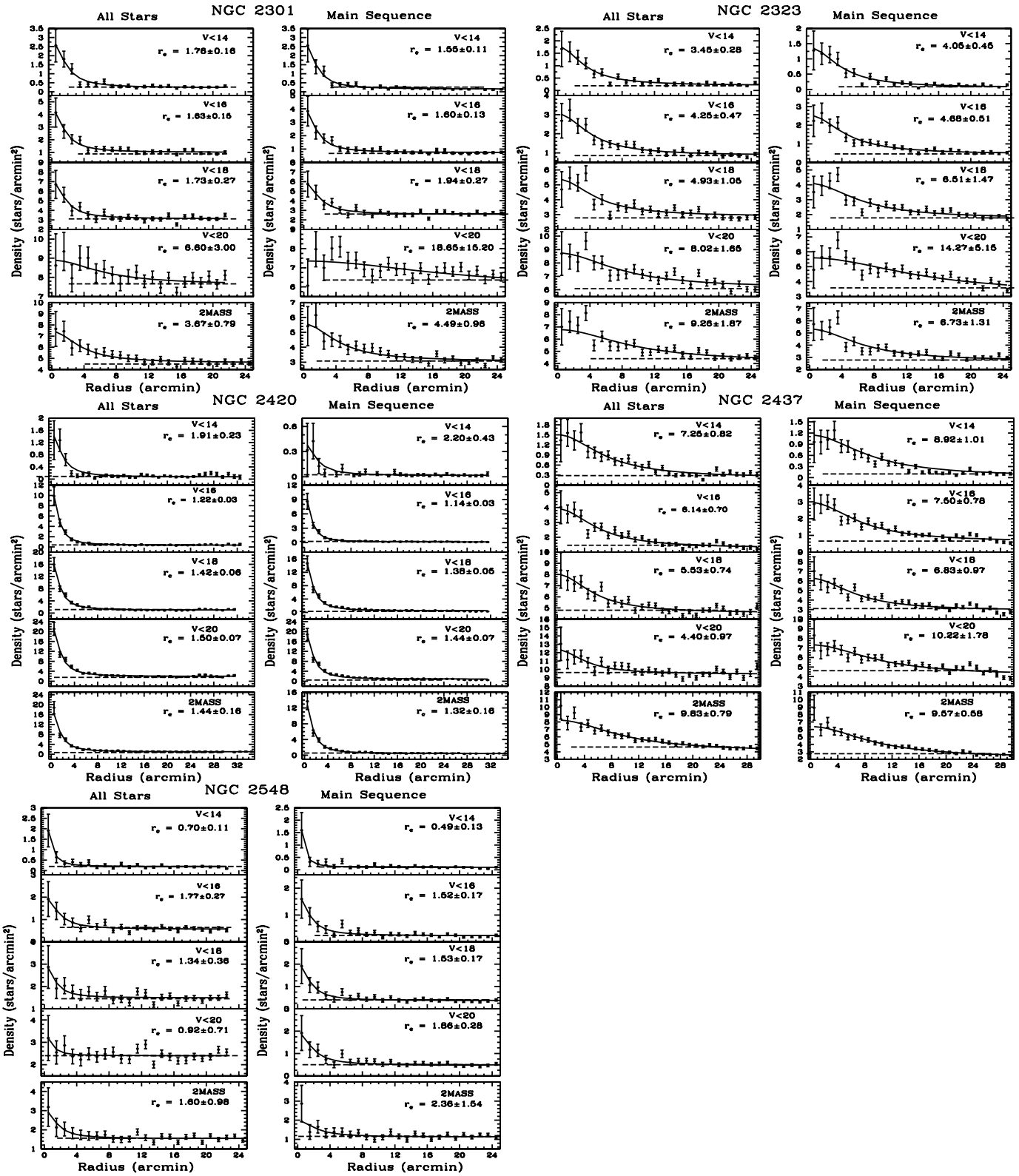

FIG. 4.—*Continued*

fit obtained by a χ^2 minimization technique is shown in Figure 4. Within uncertainties the King model (King 1962) reproduces well the radial density profiles of the clusters studied in the present work. Structural parameters obtained by fitting the King model surface density profile to the observed radial density profile of MS stars with $V < 18$ mag are given in Table 5.

The majority of the clusters indicate an increase in core radius when fainter cluster members are included in the radial density profile; however, two clusters, namely, NGC 1960 (log age $\sim$7.4) and NGC 2437 (log age $\sim$8.4), yield a smaller r_c toward fainter magnitude, whereas clusters NGC 2301 (log age $\sim$8.2) and NGC 2420 (log age $\sim$ 9.3) do not show any significant change in

TABLE 5

Structural Parameters of the Target Open Clusters, Estimated from the Projected Radial Density Profile of Main-Sequence Stars with $V \leq 18$ mag

Cluster	$\alpha_{2000.0}$	$\delta_{2000.0}$	Optical		2MASS	
			Core Radius[a]	Cluster Extent[a]	Core Radius[a]	Cluster Extent[a]
Be 62	01 01 15.5	63 56 17	2.2 (1.5)	10.0 (6.8)	2.5 (1.7)	12 (8.1)
NGC 1528	04 15 24.2	51 15 23	8.3 (2.6)	15.0 (4.8)	18.5 (5.9)	24 (7.6)
NGC 1960	05 36 20.8	34 08 31	3.2 (1.2)	14.0 (5.4)	3.8 (1.5)	21 (8.1)
NGC 2287	06 45 58.7	−20 44 09	1.4 (0.3)	12.0 (2.5)	12.7 (2.6)	16 (3.3)
NGC 2301	06 51 46.4	00 27 30	1.9 (0.5)	9.0 (2.3)	4.5 (1.1)	20 (5.1)
NGC 2323	07 02 47.4	−08 20 43	6.5 (1.8)	17.0 (4.7)	6.7 (1.9)	22 (6.1)
NGC 2420	07 38 24.8	21 34 30	1.4 (1.0)	10.0 (7.2)	1.3 (0.9)	9 (6.5)
NGC 2437	07 41 58.1	−14 49 28	6.8 (3.0)	20.0 (8.8)	9.6 (4.2)	25 (11.0)
NGC 2548	08 13 42.9	−05 46 37	1.5 (0.3)	8.0 (1.8)	2.4 (0.5)	8.0 (1.8)

Note.—Units of right ascension are hours, minutes, and seconds, and units of declination are degrees, arcminutes, and arcseconds.
[a] Values given in arcminutes, with values in parentheses in parsecs.

core radius as a function of brightness of the cluster stars. The radial stellar surface density profiles displayed in Figure 4 indicate that field star contamination is not significant up to $V \sim 18$ mag; however, it increases significantly at $V = 20$ mag. We expect that for the sample brighter than $V \sim 18$ mag field star contamination is not strong enough to smear the cluster properties and hence will have an insignificant effect in the results derived below. The poor radial surface density profile in the case of NGC 2287 is due to a lack of clustering in the object.

Recently, various authors have used Two Micron All Sky Survey (2MASS) data to study the radial structures of open clusters (Chen et al. 2004, hereafter C04; Bonatto & Bica 2005, hereafter BB05). We also used 2MASS data to obtain the radial density profile curve of the clusters studied in the present work, and the same are shown in Figure 4 (*bottom panels*). The core radius r_c and extent of the cluster $r_{\rm cl}$ of the target open clusters estimated from the projected radial density profile for MS-band stars are given in Table 5. Table 5 indicates that the r_c and $r_{\rm cl}$ obtained using the 2MASS data are larger, in some cases, than those obtained from optical data. The error in r_c obtained from 2MASS data is also relatively large in comparison to that for optical data. Various recent estimates of radii of target clusters are given in Table 6, which indicates a fair agreement between the present optical estimates and those by Nilakshi et al. (2002, hereafter N02). To study various parameters, e.g., interstellar reddening, age, or distance, in detail, we considered only those stars that are inside the cluster extent as determined from the radial density profile.

TABLE 6

Recent Estimates of Sizes of Target Clusters Available in the Literature

Name	K05		N02		C04		BB05	
	r_c	$r_{\rm cl}$	r_c	$r_{\rm cl}$	$r_{1/3}$	$r_{\rm out}$	$R_{\rm core}$	$R_{\rm lim}$
NGC 1528	8.4	26.4						
NGC 1960	5.4	16.2	3.2	15.4	5.7	7.6		
NGC 2287	9.6	30.0					4.7	30.1
NGC 2301	4.8	15.0	1.9	12.0				
NGC 2323	6.0	22.2	2.6	16.7				
NGC 2420			1.5	13.2	3.7	11.6		
NGC 2437	7.2	22.8	5.2	26.6				
NGC 2548	15.0	43.8					3.9	37.8

Note.—Sizes are in arcminutes.

4.2. *Isodensity Contours*

It is well known that the internal interaction of two-body relaxation due to encounters among member stars and external tidal forces due to the Galactic disk or giant molecular clouds influence the morphology of clusters. To study the effects of external forces on the morphology of clusters, we obtained isodensity contours for the sample of MS stars ($V \leq 18$ mag); the contours are shown in Figure 5. The isodensity contours are least-squares fitted with an ellipse to obtain the elongation of the corona of the clusters. The elongation parameter e_p is defined as $e_p = b/a$, where a and b are the semimajor and semiminor axes of the ellipse, respectively. The parameter e_p for each cluster is given in Figure 5; $e_p = 1$ indicates a spherical cluster. The fitting could not be done in the case of Be 62 and NGC 1960. However, a visual inspection of the density contours of these two clusters indicates an elongated corona of the clusters. C04 have also reported an elongated corona in the case of NGC 1960.

Figure 5 indicates that the outer regions (coronae) of six clusters are found to be elongated. The elongated morphology in the case of NGC 2287, NGC 2548 (Bergond et al. 2001, hereafter B01), NGC 1893, Be 17, and NGC 2420 (C04) have already been reported in the literature. The present results further support the elongated morphology of the coronal regions of the clusters.

4.3. *Interstellar Extinction*

The extinction toward the clusters Be 62, NGC 1960, NGC 2301, and NGC 2323 was estimated using the $(U - B,\ B - V)$ two-color diagram (TCD) shown in Figure 6. We compared the observed MS in the cluster region with the intrinsic MS to estimate the value of reddening, $E(B - V)$. In Figure 6 we show the intrinsic MS for $Z = 0.02$ by Schmidt-Kaler (1982) shifted along the reddening vector with a normal slope of $E(U - B)/E(B - V) = 0.72$. The interstellar extinction in the case of the other five clusters (NGC 1528, NGC 2287, NGC 2420, NGC 2437, and NGC 2548) was estimated using the $V/(B - V)$ or $V/(V - I)$ CMDs (cf. § 4.4). The estimated values of the $E(B - V)$ are given in Table 7, which are in good agreement with those given in the literature. Barring the cluster Be 62, all other clusters show a uniform reddening across the cluster region. The reddening in Be 62 varies from $E(B - V)_{\rm min} = 0.70$ mag to $E(B - V)_{\rm max} = 1.00$ mag. The reddening for individual stars ($V_{\rm error} \leq 0.1$ mag) with spectral type earlier than A0 has also been derived using the Q-method (Johnson & Morgan 1953).

To study the nature of the extinction law in the cluster region, we used TCDs as described by Pandey et al. (2001, 2003). TCDs

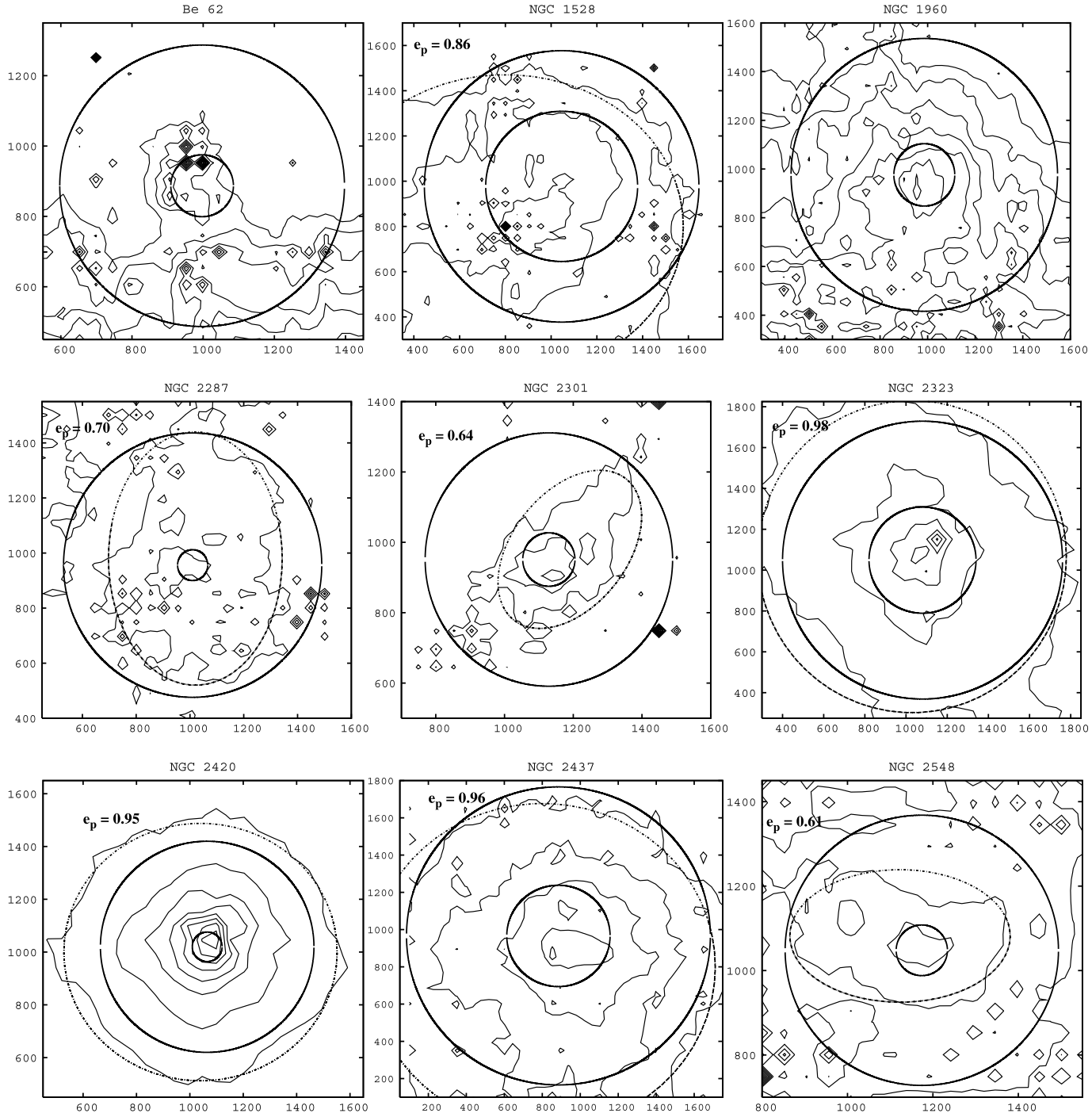

FIG. 5.— Isodensity contours drawn for the target clusters. The x- and y-axes are in pixels. The inner and outer circles represent the core and cluster radius as obtained in the present study. The dashed curve shows the least-squares fitted curve to the outer region of the clusters, and e_p is the elongation parameter (see text).

of the form $(\lambda - V)$ versus $(B - V)$, where $(\lambda - V)$ is one of the wavelengths of the broadband filters (R, I, J, H, K, L), provide an effective method for separating the influence of the normal extinction produced by the diffuse interstellar medium from that of the abnormal extinction arising within regions having a peculiar distribution of dust sizes (e.g., Chini & Wargau 1990; Pandey et al. 2000). The near-infrared (NIR) data have been taken from 2MASS. For illustration, the TCDs for the clusters Be 62, NGC 2420, and NGC 1960 are shown in Figure 7, and slopes of the distribution, $m_{\rm cluster}$, in the cases of these three clusters are given in Table 8.

The $E(\lambda - V)/E(B - V)$ values in the cluster region are estimated using the following approximate relation

$$\frac{E(\lambda - V)}{E(B - V)} = \frac{m_{\rm cluster}}{m_{\rm normal}} \left[\frac{E(\lambda - V)}{E(B - V)}\right]_{\rm normal},$$

as described by Pandey et al. (2003), where $m_{\rm cluster}$ and $m_{\rm normal}$ are the slope of the distribution in the cluster region and the slope of the theoretical MS, respectively. The slopes of the theoretical MS, $m_{\rm normal}$, obtained from the stellar models by Bertelli et al.

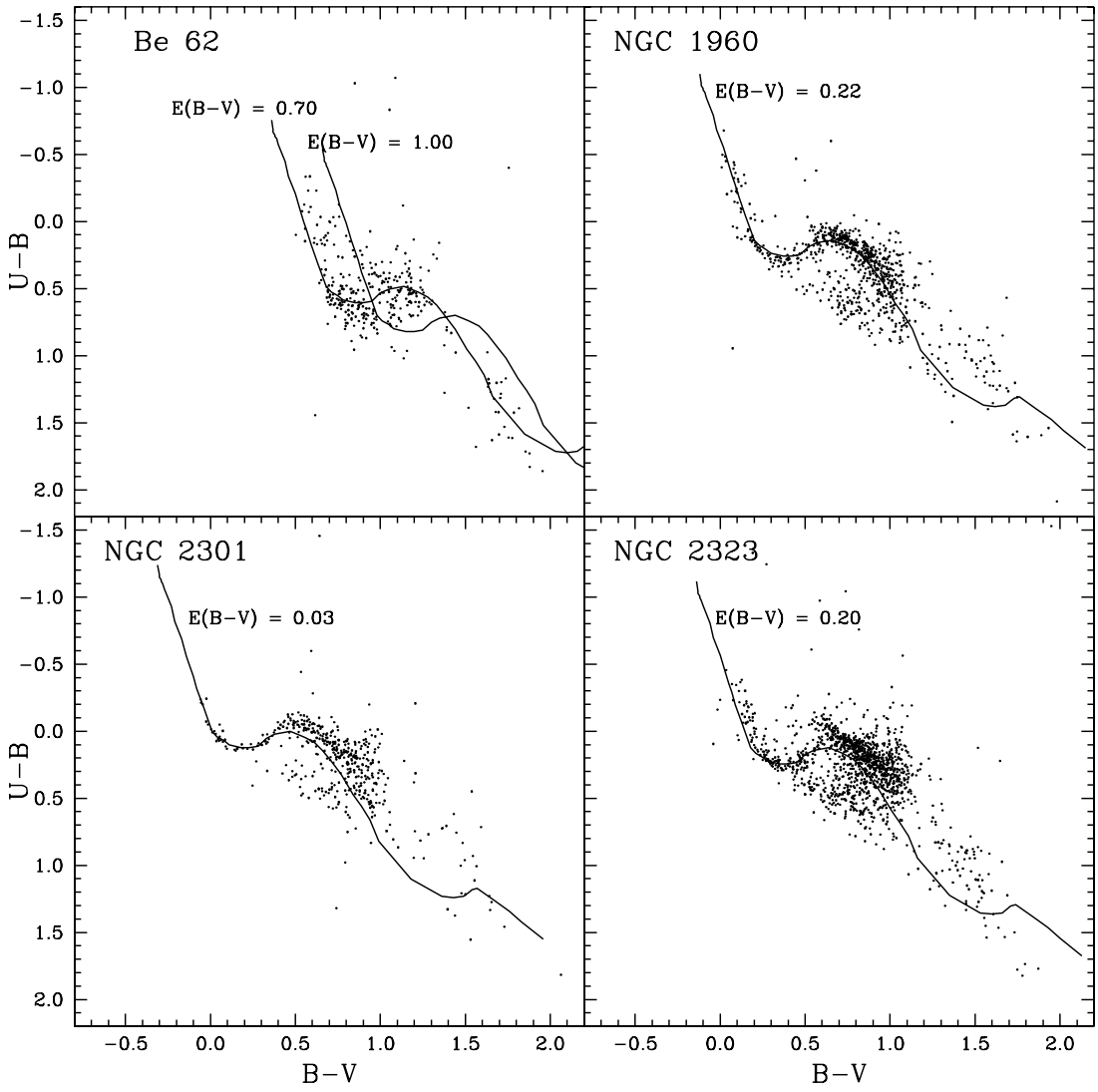

FIG. 6.—$(U-B,\ B-V)$ color-color diagram for the stars within the region $r \leq r_{\rm cl}$ of clusters Be 62, NGC 1960, NGC 2301, and NGC 2323. The solid curve represents the intrinsic MS for $Z = 0.02$ by Schmidt-Kaler (1982) shifted along the reddening vector of 0.72.

(1994), are also given in Table 8. The obtained slope $m_{\rm cluster}$ indicates that, barring Be 62 and NGC 2420, all other clusters show a normal reddening law toward the cluster region. The color excess ratios $E(\lambda - V)/E(B - V)$ for Be 62 and NGC 2420 are smaller than the normal ones, which indicates that there may be an anomalous reddening law toward these cluster regions. Since Be 62 shows a differential extinction indicating that the stars are still embedded in the parent molecular gas and dust, an anomalous reddening law is expected in the cluster region. The value of R toward the cluster Be 62 region is estimated to be 2.95 ± 0.12. However, anomalous reddening is quite surprising in the case of NGC 2420, which is an old cluster having a uniform reddening across it. Keeping the large error in mind we use a normal value of R for all the cluster regions in the ensuing discussions.

TABLE 7

THE ESTIMATED PARAMETERS OF THE TARGET CLUSTERS OBTAINED IN THE PRESENT WORK USING COLOR-COLOR DIAGRAMS AND COLOR-MAGNITUDE DIAGRAMS

Cluster	$E(B-V)$ (mag)	Log Age (yr)	Distance $(V-M_V)$	Distance (kpc)	R_G (kpc)
Be 62.....	0.70–1.00	7.2	14.0	2.32	9.98
NGC 1528.....	0.26	8.6	11.0	1.09	9.48
NGC 1960.....	0.22	7.4	11.3	1.33	9.82
NGC 2287.....	0.01	8.4	9.3	0.71	8.96
NGC 2301.....	0.03	8.2	9.8	0.87	9.25
NGC 2323.....	0.20	8.0	10.5	0.95	9.23
NGC 2420.....	0.04	9.3	12.1	2.48	10.76
NGC 2437.....	0.10	8.4	11.2	1.51	9.51
NGC 2548.....	0.03	8.6	9.5	0.77	9.02

NOTE.—To determine the galactocentric distances (R_G) to the clusters, a value of 8.5 kpc has been assumed for the galactocentric distance of the Sun.

4.4. *Color-Magnitude Diagrams, Distances, and Ages of the Clusters*

CMDs for stars lying within a cluster region, as mentioned in Table 5, are shown in Figure 8. The CMDs show a well-defined MS. Barring Be 62, other clusters manifest a uniform reddening in the cluster region, and the error in magnitude estimation is $\sim$0.05 mag for stars with $V \leq 18.0$ mag. Therefore, we can conclude that the presence of probable binaries and field stars should be the main cause for broadening of the MS in these clusters. In the case of Be 62, variable reddening in the cluster region, along with the presence of probable binaries and field stars, should be

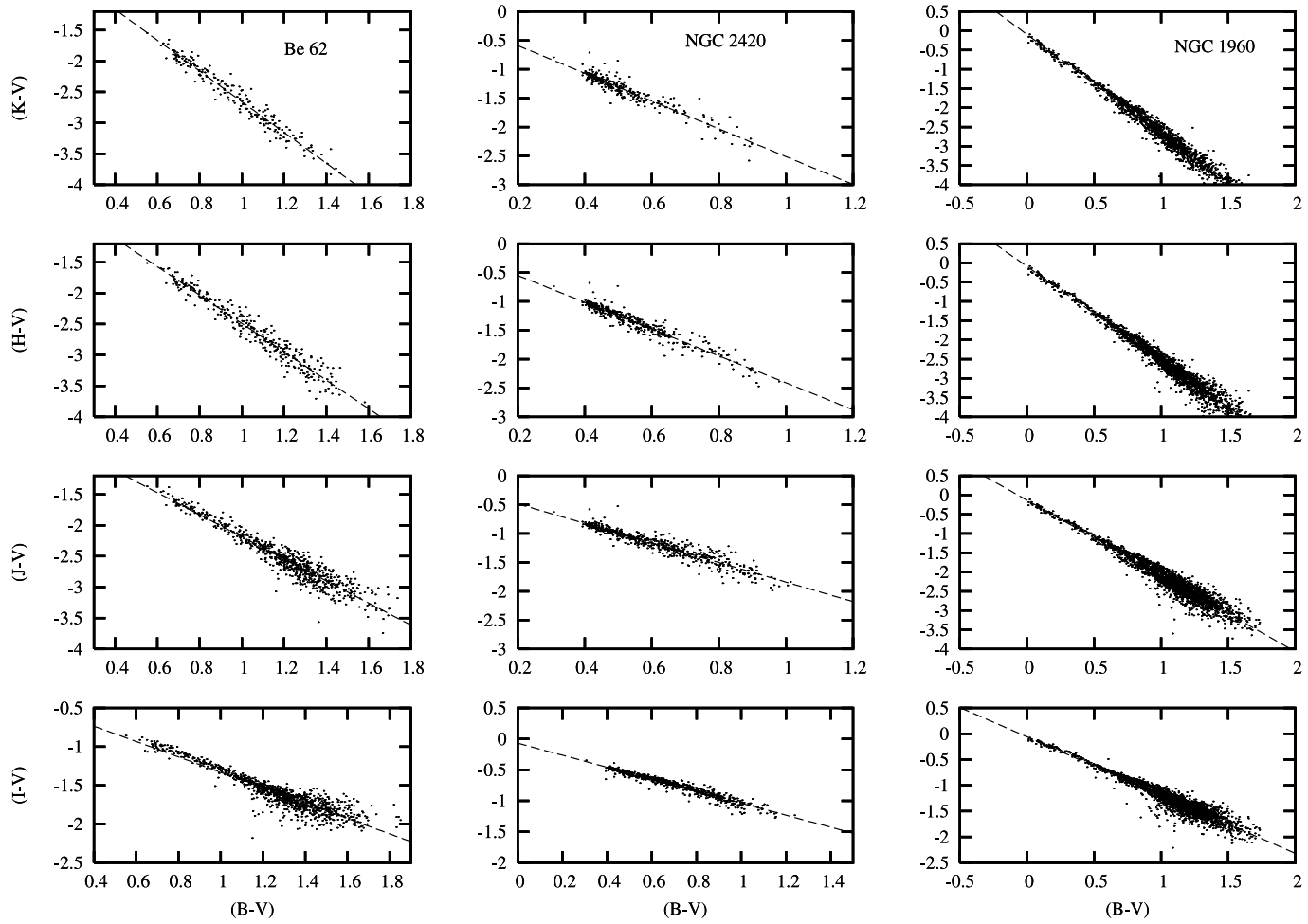

FIG. 7.—$(I - V)$, $(J - V)$, $(H - V)$, and $(K - V)$ vs. $(B - V)$ TCDs, within the cluster region ($r \leq r_{cl}$), for the clusters Be 62, NGC 2420, and NGC 1960. The dashed line shows a least-squares fit to the data.

the cause of the broad MS. It is difficult to separate field stars from the cluster stars; however, we can reduce the contamination due to field stars if we restrict the sample to the central portion of the cluster only.

We supplemented the present CCD data for some clusters with the photoelectric photometry for bright stars available in the literature, as these bright stars were saturated even in the present short-exposure frames. The distances and ages of the clusters were obtained by visual fitting of isochrones by Bertelli et al. (1994) for $Z = 0.02$ to the blue envelope of the observed MS except in the case of NGC 2420, for which we used isochrones for $Z = 0.008$, as Lee et al. (2002) have reported $Z = 0.009$ for the cluster NGC 2420. The fitted isochrones are shown in Figure 8. Since extinction is uniform in the clusters under study except Be 62, we used a mean value of $E(B - V)$ and the relations $E(U - B)/E(B - V) = 0.72$, $A_V = 3.1E(B - V)$, $E(V - R) = 0.60E(B - V)$, and $E(V - I) = 1.25E(B - V)$ to fit the theoretical isochrones to the observations. In the case of Be 62 individual reddening for stars earlier than A0 was obtained using the Q-method, and the same was applied to get the intrinsic magnitude and colors, whereas for other stars the mean reddening of the nearby stars was applied to get the intrinsic magnitude and colors. The unreddened CMDs, along with the fitted isochrones in the case of Be 62, are shown in Figure 9. The ages and distances obtained for the target clusters are given in Table 8. The $(K,\ J - K)$ CMDs for the clusters obtained from 2MASS data are shown in Figure 10. The theoretical isochrones by Bertelli et al. (1994) using the parameters obtained from the optical data

TABLE 8
SLOPES OF TCDS FOR CLUSTERS Be 62, NGC 2420, AND NGC 1960

Cluster	Radius (arcmin)	$(I - V)/(B - V)$	$(J - V)/(B - V)$	$(H - V)/(B - V)$	$(K - V)/(B - V)$
Be 62	<10	-0.99 ± 0.01	-1.78 ± 0.02	-2.29 ± 0.03	-2.49 ± 0.03
NGC 2420	<10	-0.97 ± 0.01	-1.69 ± 0.02	-2.32 ± 0.03	-2.40 ± 0.05
NGC 1960	<14	-1.13 ± 0.01	-1.97 ± 0.01	-2.44 ± 0.01	-2.56 ± 0.01
Normal value[a]	...	-1.10	-1.96	-2.42	-2.60

[a] See text.

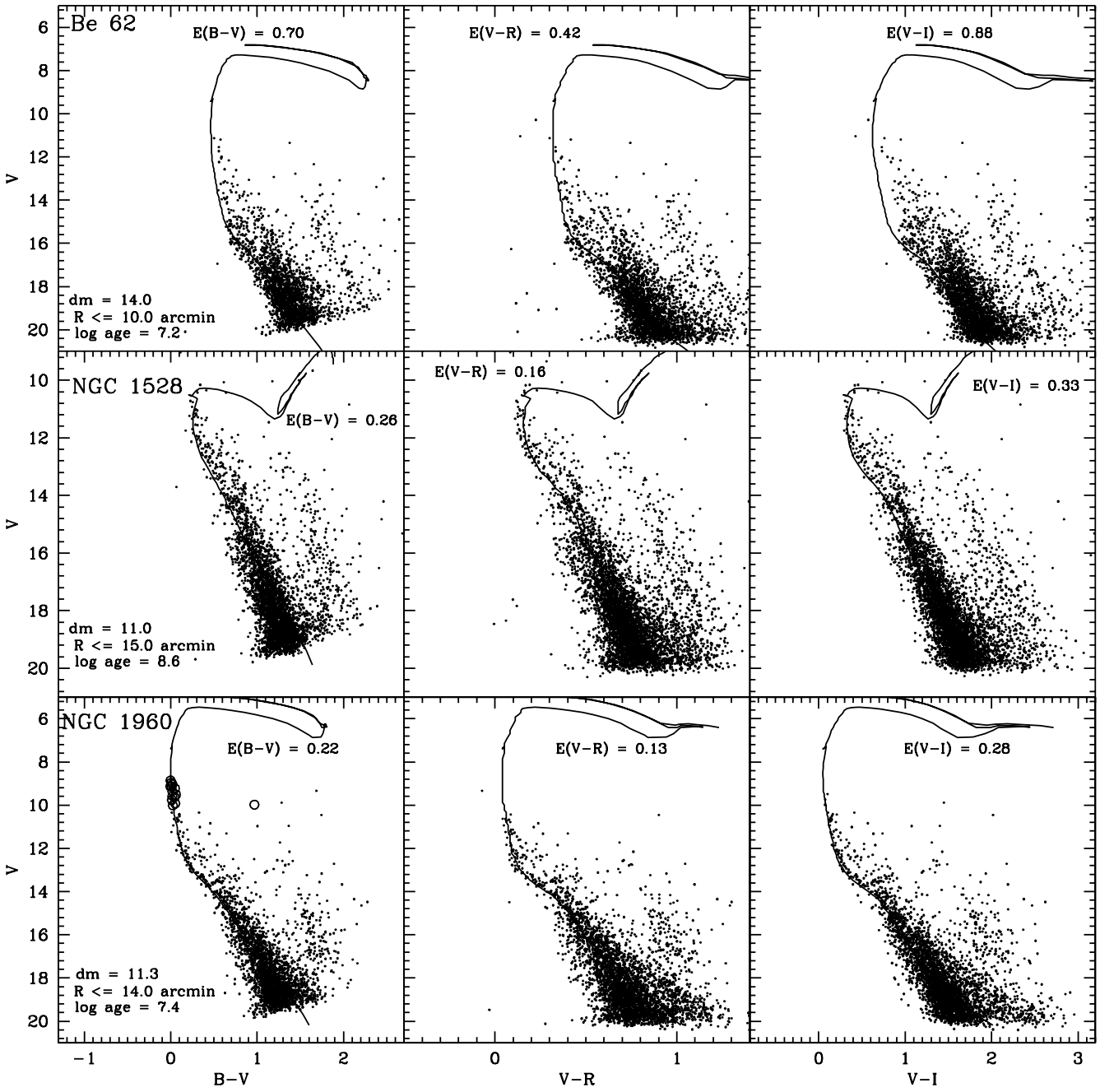

FIG. 8.— V vs. $(B-V)$, $(V-R)$, and $(V-I)$ CMDs for clusters Be 62, NGC 1528, NGC 1960, NGC 2323, NGC 2301, NGC 2287, NGC 2420, NGC 2437, and NGC 2548. The isochrones by Bertelli et al. (1994) for solar metallicity and the indicated logarithmic age are also shown. The open circles represent photoelectric data taken from the literature.

(cf. Table 7) are also plotted in Figure 10, which nicely follow the observations. A comparison of previous estimates available in the literature with the present estimates is given in Table 9.

5. RESULTS

We have determined the basic parameters of nine open clusters by analyzing the color-color diagrams and CMDs of the clusters. We assumed solar abundance for all the clusters except NGC 2420, for which the metallicity is reported to be $Z = 0.009$ by Lee et al. (2002). A discussion on individual clusters follows, in which we have compared the radii of the clusters obtained in the present study with those reported by N02, BB05, C04, and Kharchenko et al. (2005, hereafter K05). The morphological parameters of the open clusters derived by N02 and K05 are based on optical observations, whereas C04 and BB05 have used 2MASS data. In the subsequent sections we use the core radius r_c and cluster extent $r_{\rm cl}$ obtained from the present optical, photometric, and 2MASS data.

5.1. *Be 62*

The reddening $E(B-V)$, distance, and age for this cluster have been estimated as 0.86 mag, 2.05 ± 0.24 kpc, and 10 Myr by Forbes (1981) using photoelectric photometry, whereas Phelps & Janes (1994), using CCD observations, reported $E(B-V) = 0.82$ mag, a distance of 2.7 kpc, and an age of $\sim$10 Myr for this cluster.

In Figure 8 (V, $B-V$), (V, $V-R$), and (V, $V-I$) CMDs for stars within the cluster region, i.e., $r_{\rm cl} = 10'.0$ (6.8 pc), are

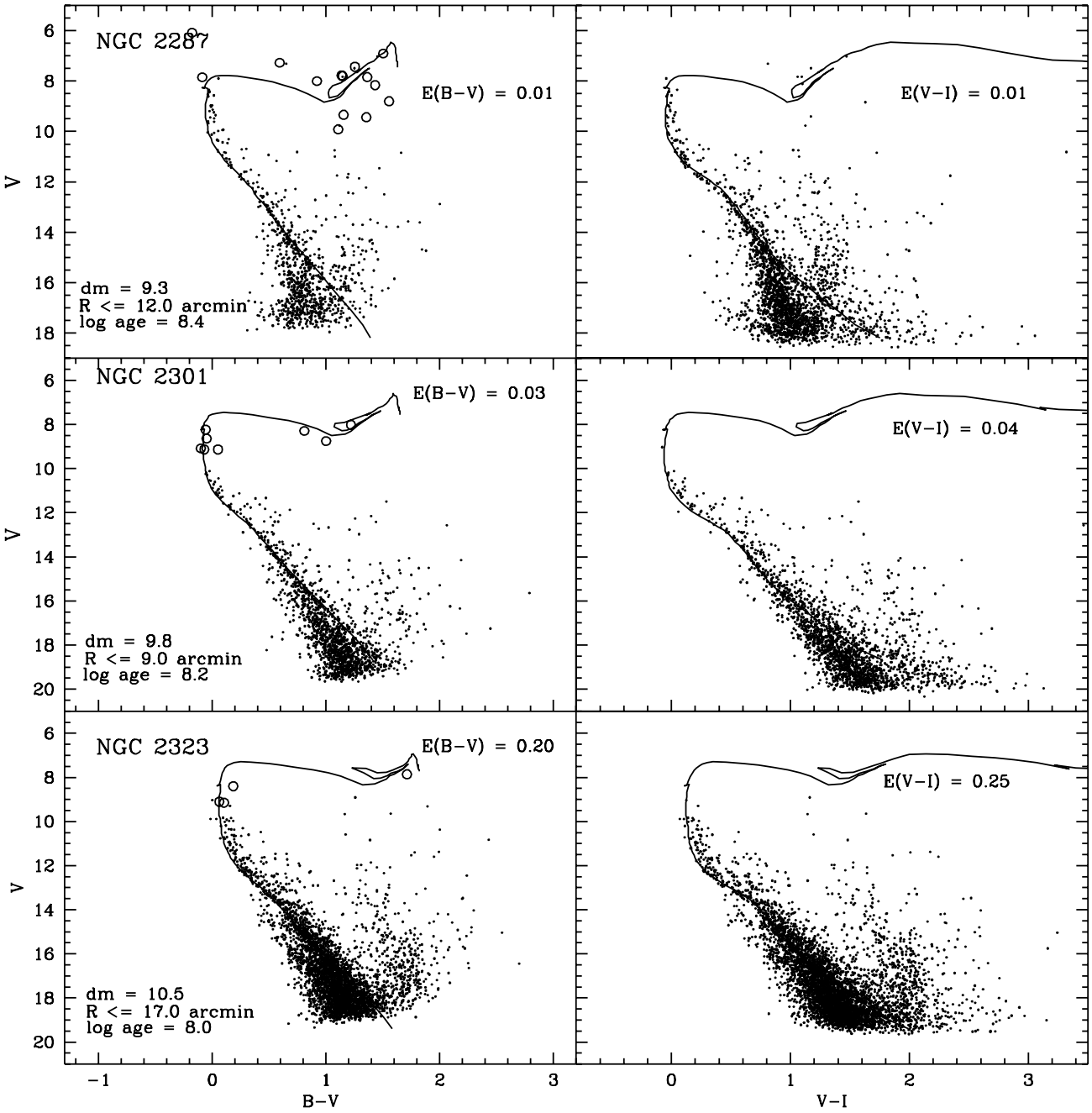

FIG. 8.—*Continued*

presented. The CMDs of Be 62 show a broad MS that should be due to variable reddening in the cluster region. To get unreddened CMDs, the reddening $E(B-V)$ for stars with spectral type A0 or earlier has been calculated using the Q-method, and these stars were dereddened individually. For the remaining stars the average reddening of nearby stars was applied. The unreddened CMDs are shown in Figure 9. To calculate V_0, a value of $R = 3.1$ is assumed. The distance and age of the cluster come out to be 2.32 kpc and 16 Myr (log age = 7.2). The distance obtained in the present work is in between the values of 2.05 and 2.70 kpc reported by Forbes (1981) and Phelps & Janes (1994), respectively.

The core of the cluster, using the optical MS data, is estimated to be $\sim 2\farcm2 \pm 0\farcm3$ (1.5 ± 0.2 pc). The 2MASS data give the value for the core as $\sim 2\farcm5 \pm 1\farcm0$ (1.7 ± 0.7 pc). The optical and 2MASS data yield the extents of the clusters as $\sim 10'$ (6.8 pc) and $\sim 12'$ (8.1 pc), respectively. The core and the coronal region of the cluster are found to be elongated.

5.2. *NGC 1528*

The radial density profile of this cluster yields an extent $r_{\rm cl} \sim 15'$ (4.8 pc) with a core radius $r_c \sim 8\farcm3 \pm 1\farcm5$ (2.6 ± 0.5 pc), which is in agreement with the value ($8\farcm4$) from K05; however, the $r_{\rm cl}$ obtained in the present work ($\sim 15'$) is significantly smaller than the value ($26\farcm4$) from K05. The radial density profile obtained using the 2MASS data is quite noisy, and it yields a significantly different value of r_c ($\sim 18\farcm5 \pm 7\farcm4$; 5.9 ± 2.4 pc).

The CMDs of the cluster within $r_{\rm cl} \sim 15'$ show a well-defined but broad MS. Since the cluster has uniform reddening, the presence of binary stars is a probable reason for the broadening of the MS. The CMDs show the turnoff of the MS, which can be fitted

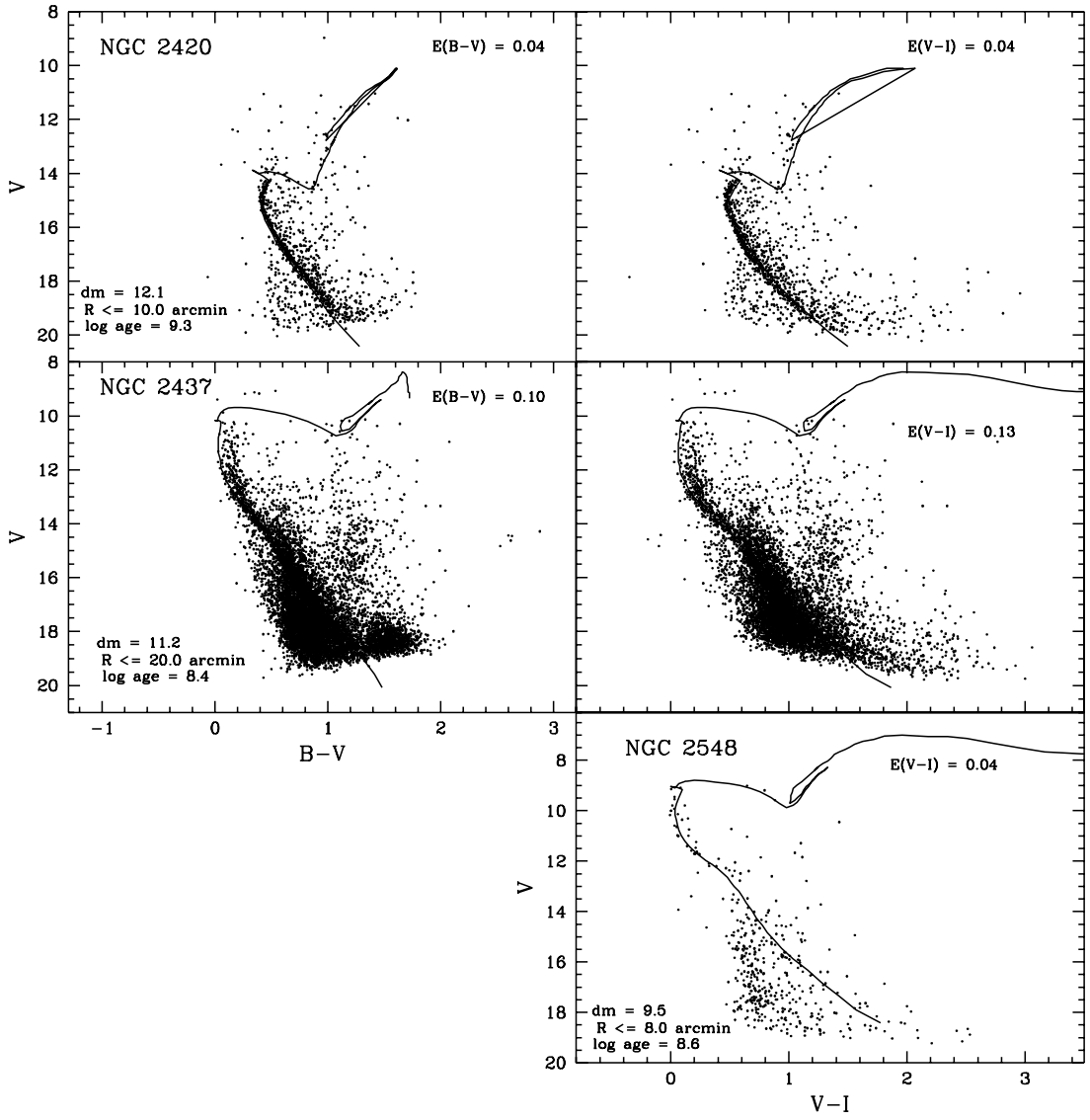

FIG. 8.—*Continued*

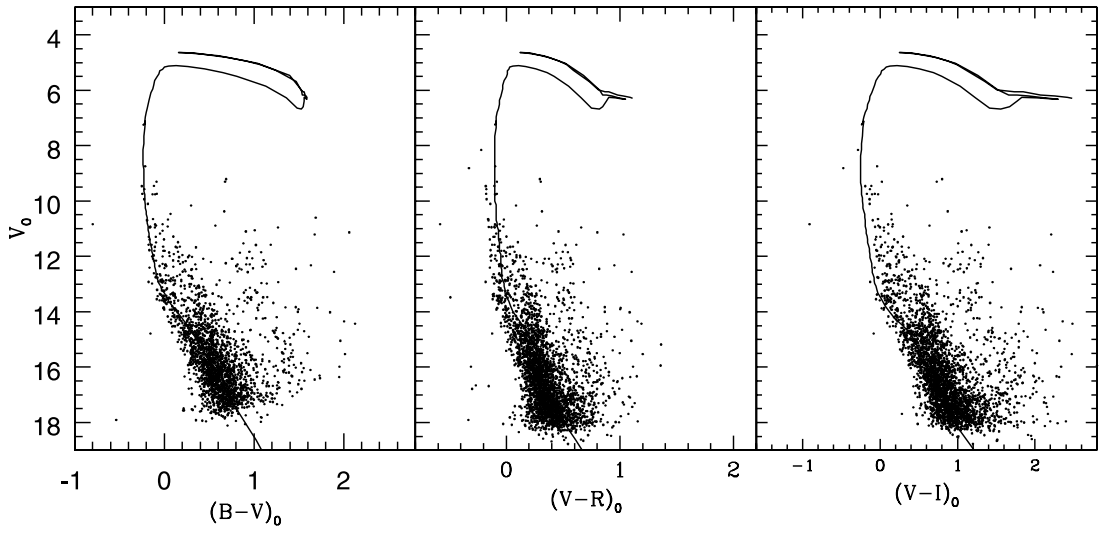

FIG. 9.—Unreddened CMDs for the cluster Be 62. The isochrone by Bertelli et al. (1994) for solar metallicity and log age = 7.2 is also shown.

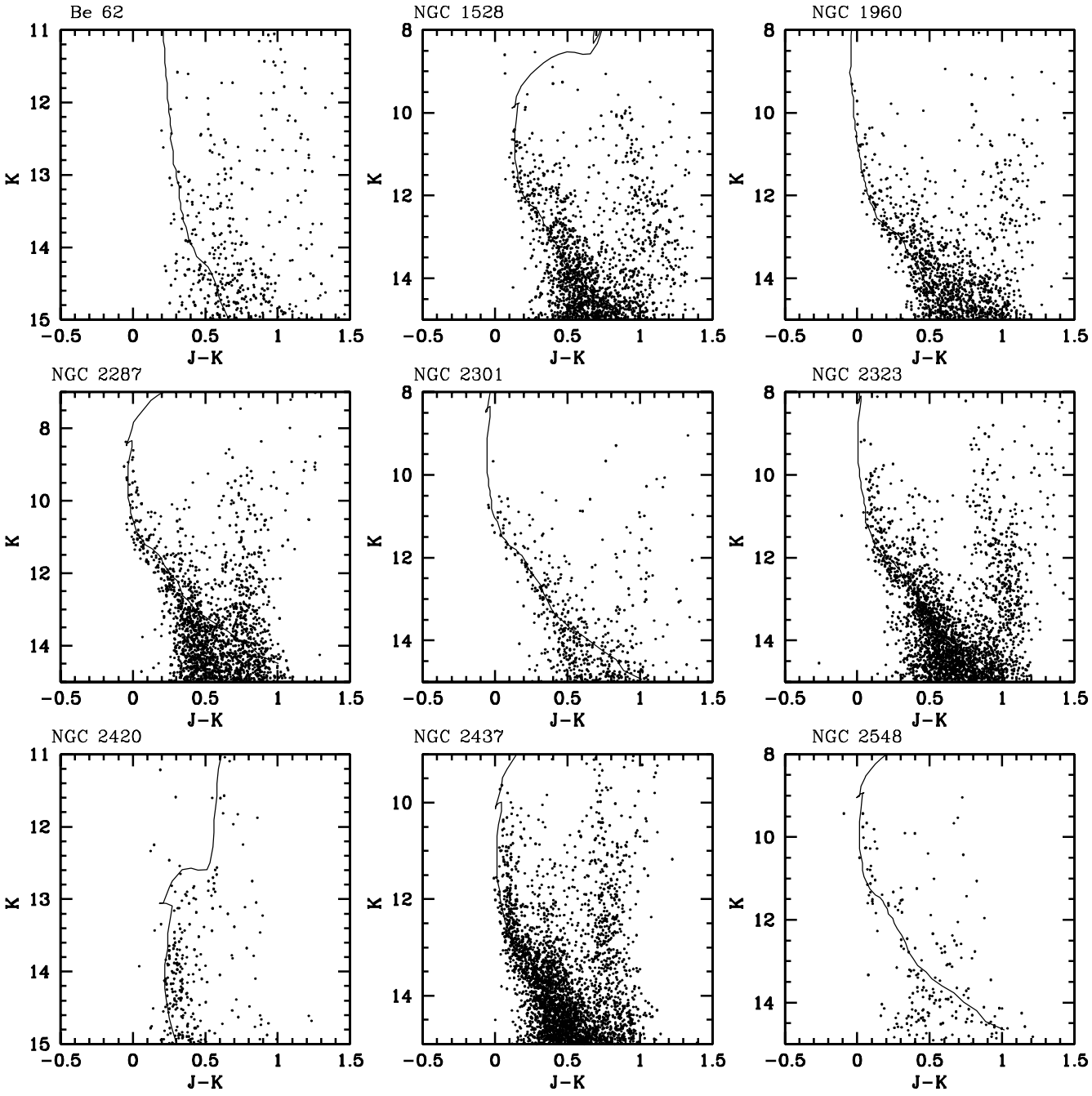

FIG. 10.—K vs. $(J-K)$ CMDs for target clusters obtained from 2MASS data. The isochrones by Bertelli et al. (1994) for the age obtained in the present work (cf. Table 8) are also shown. The values of $E(B-V)$ and the distance modulus for the clusters have been adopted from Table 8.

nicely with isochrones of log age = 8.6 (400 Myr) and $Z = 0.02$. The distance to the cluster comes out to be 1.09 kpc, which is in agreement with those distances reported in the literature. The isodensity curves shown in Figure 5 indicate that both the core and the corona have elongated morphology.

5.3. *NGC 1960 (M36)*

This cluster situated in the constellation Auriga is reported to have a diameter of 10′ (Lynga & Palous 1987). Sanner et al. (2000) reported a distance modulus $(m-M)_0 = 10.6 \pm 0.2$ mag (1318 ± 120 pc), reddening $E(B-V) = 0.25 \pm 0.02$ mag, age $= 16^{+10}_{-5}$ Myr, and metallicity $Z = 0.02$ for the cluster.

The CMDs of NGC 1960 show a well-defined narrow MS. By fitting the isochrones for log age = 7.4 (25 Myr) to the stellar distribution in the CMDs using $E(B-V) = 0.22$ mag, we obtained a distance modulus $(m-M)_V = 11.3$ mag, corresponding to a true distance modulus $(m-M)_0 = 10.62$ mag, or a distance of 1.33 kpc. The estimated age, distance, and reddening in the cluster region are in good agreement with the values obtained in earlier studies (e.g., Sanner et al. 2000).

The core radius ($r_c \sim 3\farcm2 \pm 0\farcm5$; 1.2 ± 0.1 pc) and cluster extent ($r_{\rm cl} \sim 14'$; 5.4 pc) obtained in the present study are in good agreement with the values obtained by N02 ($r_c \sim 3\farcm2$, $r_{\rm cl} \sim 15\farcm4$). The core radius ($r_c \sim 5\farcm4$) obtained by K05 is larger than the present value. The cluster extent ($r_{\rm cl} \sim 14'$) obtained in the present work is in agreement with the value ($\sim$16.′2) from K05, whereas it is larger than that ($\sim$7.′6) reported by C04. From 2MASS data, we obtained $r_c \sim 3\farcm8 \pm 0\farcm6$ (1.5 ± 0.2 pc) and

TABLE 9
Comparison of Estimates Available in the Literature with the Present Estimates

Cluster	Observations[a]	$E(B-V)$ (mag)	Distance (pc)	Age (yr)	Reference
Be 62	pe	0.86	2050 ± 240	10^7	Forbes (1981)
	CCD	0.82	2704	10^7	Phelps & Janes (1994)
	CCD	0.70	2320	1.6×10^7	Present work
NGC 1528	pg	0.28	603	4×10^8	Francic (1989)
	CCD	0.26	1090	4×10^8	Present work
NGC 1960	CCD	0.25 ± 0.02	1318 ± 120	$16^{+6}_{-5} \times 10^6$	Sanner et al. (2000)
	CCD	0.22	1330	2.5×10^7	Present work
NGC 2287	pg	0.00	661	2×10^8	H61
				1.7×10^8	Barbaro et al. (1967)
	pe	0.03	758		Eggen (1974)
	pe			8×10^7	Eggen (1975)
	pe	0.01 ± 0.03	630	6.0 ± 10^7	Feinstein et al. (1978)
	pe		740	10^8	Eggen (1981)
	DDO	0.07 ± 0.02	752	$(1.1 \pm 0.4) \times 10^8$	Pastoriza & Ropke (1983)
	pe	0.00	675		Ianna et al. (1987)
	pe	0.064 ± 0.042	700	2×10^8	Harris et al. (1993)
	CCD	0.01	710	2.5×10^8	Present work
NGC 2301	pe	0.04	840		Nissen (1988)
	pg	0.04	794		Mohan & Sagar (1988)
		0.05	692	2×10^8	Napiwotzki et al. (1991)
	DDO	0.04	855		Twarog et al. (1997)
	CCD	0.05	832	2.5×10^8	Kim et al. (2001)
	CCD	0.03	870	1.6×10^8	Present work
NGC 2323	pg		780–860		Trumpler (1930)
	pg		500–800		Shapley (1930)
	pg		675		Collinder (1931)
	pg		520		Rieke (1935)
	pg	0.30	1210		Cuffey (1941)
	pe	0.20–0.26	1170		H61
	pg			6×10^7	Barbaro et al. (1969)
	pg	0.33	995	1.4×10^8	Mostafa et al. (1983)
		0.04	750	$(1-1.4) \times 10^8$	Lynga (1984)
	pe	0.25	931	10^8	Claria et al. (1998)
	CCD	0.22	1000	1.3×10^8	Kalirai et al. (2003)
	CCD	0.20	950	10^8	Present work
NGC 2420	pe and pg		2900	1.2×10^9	Sarma & Walker (1962)
	pg	0.01	2400		West (1967)
	pg			10^9	Cannon & Lloyd (1970)
	pg and pe	0.02	1905 ± 11	$(3.3 \pm 0.5) \times 10^9$	McClure et al. (1974)
	pg	0.02	1900	4×10^9	McClure et al. (1978)
	CCD	0.05	2450	$(3.4 \pm 0.6) \times 10^9$	Anthony-Twarog et al. (1990)
	CCD	0.05	2450	2×10^9	Lee et al. (2002)
	CCD	0.04	2480	2×10^9	Present work
NGC 2548	pe	0.04	630		Pesch (1961)
	CCD	0.03	770	4×10^8	Present work

[a] Detector used: (pe) photoelectric; (pg) photographic; (CCD) charge-coupled device; (DDO) David Dunlop Observatory photometric system.

$r_{\rm cl} \sim 21'$ (8.1 pc). The core of the cluster is rather spherically symmetric, whereas the outer region of the cluster clearly shows the effect of external forces.

5.4. *NGC 2287 (M41)*

Despite being a bright cluster, no CCD photometry is available for this cluster. This cluster has been studied for proper motion (Ianna et al. 1987), radial velocity (Amieux 1988), and spectroscopic properties (Harris et al. 1993). Battinelli et al. (1994) and B01 have reported $R_{\rm lim} = 4.0$ pc ($19'$) and $R_{\rm tidal} = 4.1$ pc ($20.'3$), respectively, for the cluster. K05 have reported $r_c \sim 9.'6$ and $r_{\rm cl} \sim 30'$. BB05 have estimated $R_{\rm core} = 1.1$ pc ($4.'7$) and $R_{\rm lim} = 7.0$ pc ($30.'1$). In the present study we found that optical data for brighter limiting visual magnitudes ($V \sim 14$ mag) and fainter limiting magnitudes ($V \leq 18$ mag) were yielding quite different values for the morphology of the cluster. For the brighter sample we obtained $r_c \sim 5.'5 \pm 0.'9$ (1.1 ± 0.2 pc) and $r_{\rm cl} \sim 17'$ (3.5 pc), whereas for the sample with $V \leq 18$ mag these values were estimated as $\sim 1.'4 \pm 0.'3$ (0.3 ± 0.2 pc) and $\sim 12'$ (2.5 pc), respectively. The radial density profile for 2MASS data is quite noisy, with $r_c \sim 12.'7 \pm 3.'8$ (2.6 ± 0.8 pc) and $r_{\rm cl} \sim 16'$ (3.3 pc). For further study of the cluster, we assumed $r_{\rm cl} \sim 12'$ (2.5 pc). The morphology of the cluster indicates that both the central region and outer region are elongated. The center coordinates for the cluster reported by B01 are shifted $15'$ southwest of the "classical" coordinates given in WEBDA. However, BB05 found the same coordinates for the center as given in WEBDA, whereas in the present work we find a center for the cluster shifted toward the north of the center as given in WEBDA.

The CMDs of the clusters show a very well defined MS along with a red giant clump. The distance and age for the cluster are estimated to be 0.71 kpc and 250 Myr (log age = 8.4), which are in agreement with recent findings.

5.5. *NGC 2301*

A comparison of the theoretical isochrones with the observations yields a distance modulus $(m - M)_V = 9.8$ mag, which corresponds to a true distance modulus $(m - M)_0 = 9.71$ mag, or a distance of 0.87 kpc, and an age of 160 Myr (log age = 8.2) for the cluster. The age, distance, and reddening toward the cluster region obtained in the present work are in good agreement with those reported in the literature.

The estimated core radius ($r_c \sim 1.'9 \pm 0.'3$; 0.5 ± 0.1 pc) is in good agreement with the value ($r_c \sim 1.'9$; 0.5 pc) from N02, whereas it is significantly smaller than the $r_c \sim 4.'8$ by K05. The extent of the cluster ($\sim 9'$; 2.3 pc) obtained in the present work is smaller than that reported by N02 ($12'$; 3.0 pc) and K05 ($\sim 15'$). Here it is worthwhile to mention that the core radius ($r_c \sim 4.'5 \pm 1.'0$; 1.1 ± 0.2 pc) and cluster extent ($r_{\rm cl} \sim 20'$; 5.1 pc) obtained from the 2MASS data are almost double those values obtained from the optical observations. The core and coronal region of the cluster NGC 2301 are found to be highly elongated, indicating a strong effect of external forces on the cluster.

5.6. *NGC 2323 (M50)*

The distribution of MS stars with $V \leq 18$ mag yields $r_c \sim 6.'5 \pm 1.'5$ (1.8 ± 0.4 pc) and $r_{\rm cl} \sim 17'$ (4.7 pc). The core radius obtained in the present study is larger than that obtained by N02 ($2.'6$) but in agreement with that obtained by K05 ($6'$). The extent of the cluster is in agreement with that reported by N02 ($16.'7$); however, it is smaller than that reported by K05 ($\sim 22.'2$). The 2MASS data yield $r_c \sim 6.'7 \pm 1.'3$ (1.9 ± 0.4 pc) and $r_{\rm cl} \sim 22'$ (6.1 pc). The radial density profile derived from optical and 2MASS data thus gives a comparable core radius. The core and the coronal region of the cluster are found to be spherical.

The cluster NGC 2323 shows a well-defined MS toward the brighter end ($V \leq 15$ mag). The effect of photometric error becomes significant toward the fainter end. A comparison of the observations with the theoretical isochrones yields a distance of 0.95 kpc and an age of $\sim$100 Myr (log age = 8.0) for the cluster.

5.7. *NGC 2420*

The *BV* and *VI* CCD photometry for the cluster NGC 2420 were carried out by Anthony-Twarog et al. (1990) and Lee et al. (2002), respectively. Leonard (1988), using the star counts from the Palomar Sky Survey, reported a quite large extent of $\sim 20'$ for the cluster. In the present work we find that optical data and 2MASS data indicate a radial extent of the cluster of $\sim 10'$ (7.2 pc) and $\sim 9'$ (6.5 pc), respectively, which are in fair agreement with those reported by C04 ($\sim 11.'6$) but smaller than those reported by N02 ($\sim 13.'2$). The core radius is estimated to be $1.'4 \pm 0.'1$ (1.0 ± 0.1 pc), which is in agreement with that obtained by N02 ($1.'5$). 2MASS data also yield nearly the same core radius, $\sim 1.'3 \pm 0.'2$ (0.9 ± 0.1 pc). The isodensity curves indicate a rather spherical core and coronal regions of the cluster. C04 have obtained a spherical core with an elongated coronal region of the cluster.

The CMDs within the cluster region displayed in Figure 8 show a well-defined MS. As can be seen in the CMDs, the contamination due to field stars is almost negligible. The CMDs manifest a sequence of evolved stars that is nicely reproduced by the theoretical isochrones for $Z = 0.008$ and log age = 9.3 (2 Gyr).

The distance to the cluster is estimated to be 2.48 kpc, which is in good agreement with the values reported by Anthony-Twarog et al. (1990), Lee et al. (2002), and West (1967), whereas the distance reported by McClure et al. (1974) is 1.9 kpc. Because of its age and metallicity, NGC 2420 is an important object for testing theoretical stellar evolution models.

TABLE 10
PARAMETERS FOR TARGET CLUSTERS FOR A MASS-LIMITED SAMPLE WITH $M_V \leq 7$ mag

Name	Core[a]	Cluster[a]	f_0[b]
Be 62[c]	2.8 (1.9)	14.0 (9.5)	3.0 (6.6)
NGC 1528	8.3 (2.6)	15.0 (4.8)	1.7 (16.9)
NGC 1960	3.5 (1.4)	14.0 (5.4)	2.8 (18.7)
NGC 2287	1.0 (0.2)	12.0 (2.5)	2.2 (51.6)
NGC 2301	1.7 (0.4)	9.0 (2.3)	3.9 (60.9)
NGC 2323	7.2 (2.0)	17.0 (4.7)	2.5 (32.7)
NGC 2420	1.4 (1.0)	10.0 (7.2)	19.8 (38.1)
NGC 2437	8.3 (3.6)	20.0 (8.8)	3.5 (18.1)
NGC 2548	1.7 (0.4)	8.0 (1.8)	1.4 (27.9)

[a] Values given in arcminutes, with values in parentheses in parsecs.
[b] Central density of clusters, given in stars arcmin^{-2}, with values in parentheses in stars pc^{-2}.
[c] This sample is for $M_V \leq 6$ mag.

5.8. *NGC 2437 (M46)*

The star-count peak obtained in the present work is shifted by $\sim 3'$ east and $\sim 1'$ south from the center coordinates given in WEBDA. The radial density profile obtained for optical, as well as 2MASS, data shows a well-defined distribution of stellar density around the center of the cluster. However, the extent of the cluster obtained for the two distributions differs. The $r_{\rm cl}$ was estimated to be $\sim 20'$ (8.8 pc) and $25'$ (11.0 pc) for the optical and 2MASS data, while the corresponding values of r_c are $6.'8 \pm 1.'0$ (3.0 ± 0.4 pc) and $9.'6 \pm 0.'6$ (4.2 ± 0.3 pc), respectively. The values of r_c reported by K05 and N02 are $7.'2$ and $5.'2$, respectively. The corresponding $r_{\rm cl}$ values are $22.'8$ and $26.'6$, respectively. The core of the cluster is elongated, whereas the corona of the cluster is found to have spherical symmetry.

The (V, $B - V$) and (V, $V - I$) CMDs for the cluster indicate a broad and well-defined MS. The effect of field star contamination and errors is clearly visible toward the fainter end ($V >$ 15 mag). A few stars in the red giant clump region can also be noticed. Using $E(B - V) = 0.10$ mag we obtain a distance of $\sim$1.51 kpc and an age of $\sim$250 Myr (log age = 8.4) for the cluster. Since the cluster is of intermediate age and there is no indication of parental molecular gas and dust, the broad MS may be due to the presence of binary stars.

5.9. *NGC 2548 (M48)*

The point of maximum stellar density, i.e., the adopted center of the cluster, is found south ($\sim 1.'6$) of the center given in WEBDA. The center reported by BB05 is in excellent agreement with that obtained in the present work. However, B01 obtained the center of this cluster farther south ($\sim 1.'4$) than the coordinates obtained in the present work. The extent of the cluster is reported to be 4.8 pc ($21.'5$) and 8.8 pc ($37.'8$) by B01 and BB05, respectively. K05 have reported a significantly larger value ($43.'8$) for the cluster extent. The core radius r_c is reported as $3.'9 \pm 0.'9$ (0.9 ± 0.2 pc) by BB05, whereas K05 reported a significantly larger value for the core, $r_c \sim 15'$. In the present work we found $r_c \sim 1.'5 \pm 0.'2$ (0.3 ± 0.1 pc) and $\sim 2.'4 \pm 1.'5$ (0.5 ± 0.3 pc) for the optical and 2MASS data respectively, whereas the extent of the cluster for both of the samples is found to be $\sim 8'$ (1.8 pc). The elongated morphology of the coronal region of the cluster

TABLE 11
PARAMETERS OF PREVIOUSLY STUDIED CLUSTERS

Name	Log Age (yr)	Distance (kpc)	R_G (kpc)	Core Radius[a]	Cluster Radius[a]	Limiting Magnitude[b]	Reference
NGC 663	7.2	2.4	10.19	3.9 (2.7)	17.5 (12.2)	4.6	1
NGC 1912	8.5	1.4	9.89	4.5 (1.8)	14.0 (5.7)	6.5	2
NGC 7654	8.2	1.4	9.12	3.8 (1.6)	11.7 (4.8)	4.5	3
NGC 654	7.3	2.4	10.18	0.9 (0.6)	3.7 (2.6)	5.3	1
NGC 1907	8.5	1.8	10.33	2.0 (1.1)	6.0 (3.1)	5.0	2
King 5	9.0	1.9	10.09	0.8 (0.4)	2.8 (1.6)	5.0	4
King 7	8.8	2.2	10.46	1.1 (0.7)	2.9 (1.9)	3.4	4
Be 20	9.7	9.0	17.11	0.6 (1.6)	2.5 (6.6)	3.9	4

[a] Values given in arcminutes, with values in parentheses in parsecs.
[b] Upper limit for M_V.
REFERENCES.—(1) Pandey et al. 2005; (2) Pandey et al. 2006; (3) Pandey et al. 2001; (4) Durgapal & Pandey 2001.

indicates that the cluster structure has been affected by a significant amount of external forces.

The cluster shows a well-defined narrow MS in the (V, $V - I$) CMD with a few evolved stars on the giant branch. The shape of the turnoff point is that of a typical intermediate-age open cluster and can be nicely explained by an isochrone with $Z = 0.02$ and age ~400 Myr (log age = 8.6). The distance to the cluster is estimated to be 0.77 kpc.

6. DISCUSSION AND SUMMARY

6.1. *The Evolution of the Cores and Coronae of Clusters*

The isodensity curves shown in Figure 5 indicate that the coronal regions of the six clusters show an elongated morphology. The youngest cluster of the present sample, Be 62 (log age = 7.2), has an elongated core, whereas NGC 1960 (log age = 7.4) has a somewhat spherical core. On the other hand, the core of the cluster NGC 2548 (log age = 8.6) shows an elongated morphology, whereas the core of NGC 2420, the oldest cluster in the present sample (log age = 9.3) shows rather a spherical symmetry. C04 have also reported a spherical core in the case of NGC 2420. On the basis of the present small homogeneous data sample it is not possible to establish any correlation between age and shape of the core. However, C04 found that the core tends to circularize as a star cluster ages. It seems that initial morphology of the open cluster at the time of formation of the cluster is governed by the initial conditions in the parent molecular clouds (C04), because the observed shapes of molecular cloud cores also show highly elongated morphology (Curry 2002; Gutermuth et al. 2005). C04 suggested that the later evolution of the cluster may be governed by both internal gravitational interaction and external tidal forces.

Danilov & Seleznev (1994) showed that the parameters ζ ($=R_1/R_2$) and μ ($=N_1/N_2$) follow the relationship $\zeta \propto \mu^{0.35}$, where R_1 and R_2 are the radii of the cluster core and halo and N_1 and N_2 are the number of stars in the core and halo. This relationship may be caused by an approximate equality between the rates of transfer of stars from the core to the corona and vice versa as a result of stellar encounters (Danilov 1997). In order to study the

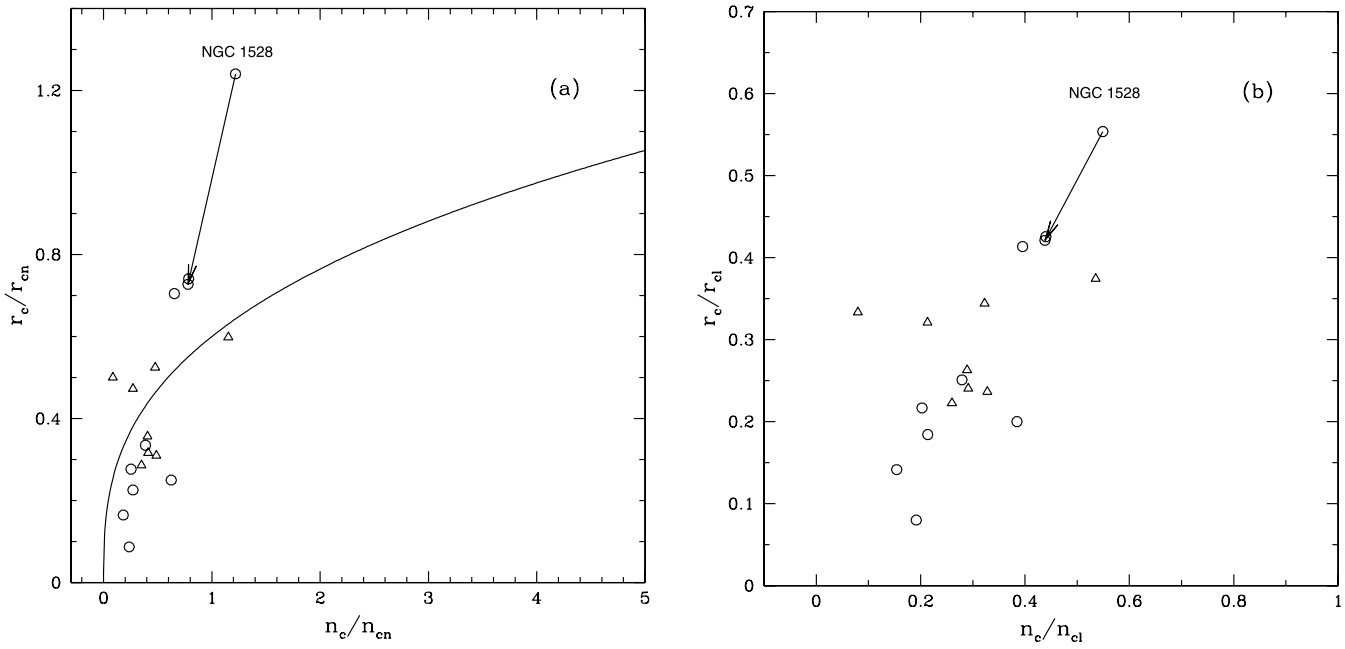

FIG. 11.—(*a*) The r_c/r_{cn} vs. n_c/n_{cn} diagram and (*b*) the r_c/r_{cl} vs. n_c/n_{cl} diagram for the clusters. The circles and triangles represent data taken from the present study and previous studies, respectively. The values r_c, r_{cn} ($=r_{cl} - r_c$), and r_{cl} represent core radius, corona size, and cluster extent, respectively, and n_c, n_{cn}, and n_{cl} represent the number of stars in the core, corona, and entire cluster, respectively. The solid curve represents the relation $r_c/r_{cn} \propto (n_c/n_{cn})^{0.35}$ (cf. § 6). The arrow indicates the revised location of NGC 1528 (see text).

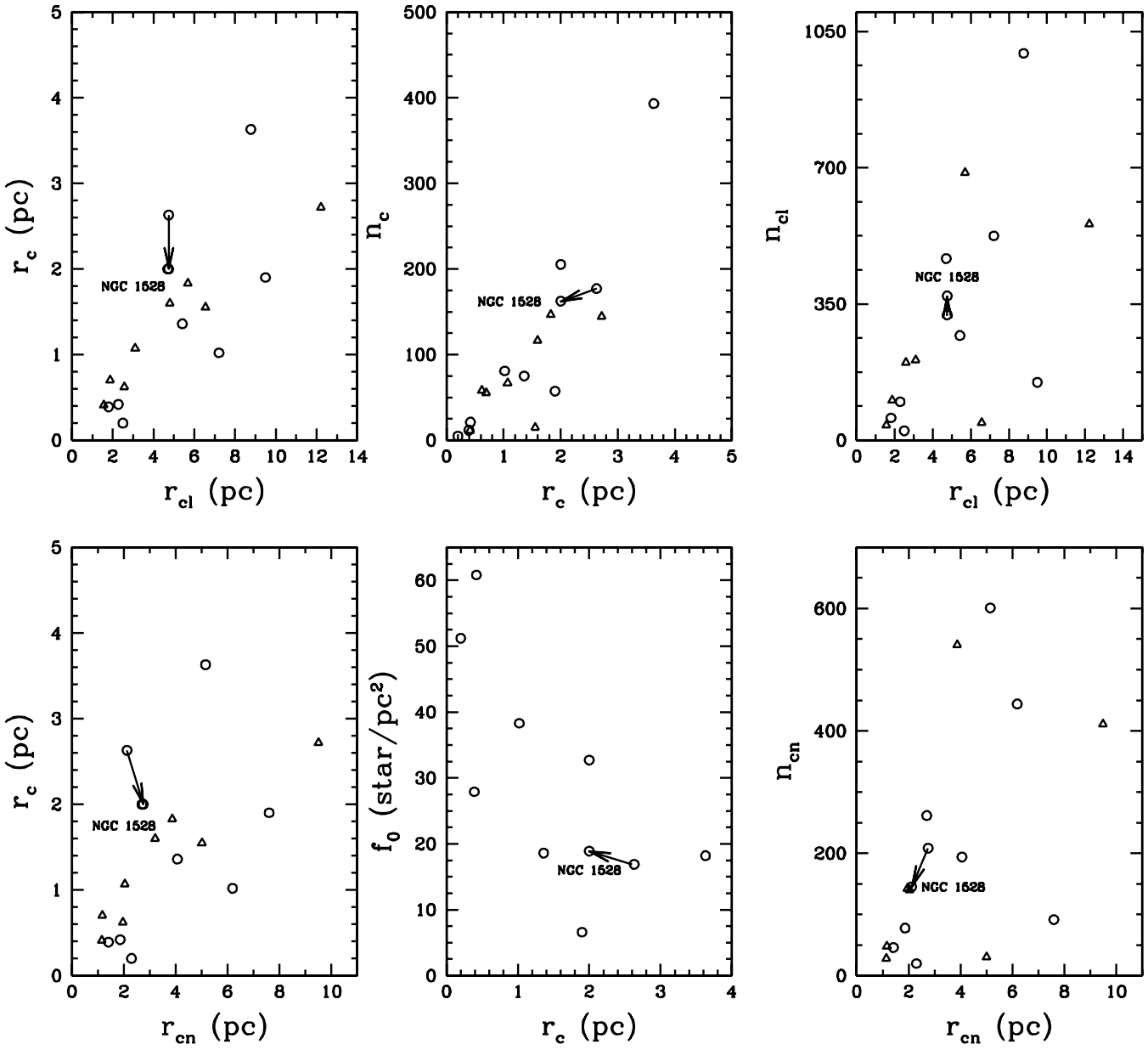

FIG. 12.—Correlation between various structural parameters of the clusters. The symbols are the same as in Fig. 11.

core-corona structure we selected a mass-limited sample, since the evolution of clusters, their stability, and their parameters depend on the mass of the cluster (e.g., Pandey et al. 1991; BB05). We estimated various parameters for the target clusters for a mass-limited sample with $M_V \leq 7$ mag, and these are given in Table 10. In the case of Be 62, it is not possible to estimate the parameters for $M_V \leq 7$ mag ($V \leq 21$ mag); we used parameters obtained for $V \leq 20$ mag ($M_V \leq 6$ mag) for further analysis. Data for a few clusters studied earlier by us have been taken from the literature, and relevant parameters for the clusters are given in Table 11. In Figure 11 we plot $r_c/r_{\rm cn}$ versus $n_c/n_{\rm cn}$ and $r_c/r_{\rm cl}$ versus $n_c/n_{\rm cl}$ diagrams for the target clusters, where r_c, $r_{\rm cn}$ ($=r_{\rm cl} - r_c$), and $r_{\rm cl}$ represent the core radius, the size of the corona, and the cluster extent, respectively, and n_c, $n_{\rm cn}$, and $n_{\rm cl}$ represent the number of stars in the core, corona, and cluster, respectively. Figure 11*a* indicates that the clusters under study except NGC 1528 follow the relation $r_c/r_{\rm cn} \propto (n_c/n_{\rm cn})^{0.35}$, as suggested by Danilov & Seleznev (1994). The anomalous location of NGC 1528 in Figure 11 is probably due to the large error in estimating the core radius because of the noisy radial density profile. If we take the core radius obtained from all star radial density profiles as shown in Figure 4, the cluster follows the expected relation shown in Figure 11. Danilov & Seleznev (1994) carried out simulations of isolated cluster dynamics and found that the parameters ζ and μ obtained from simulations also follow the relation $\zeta \propto \mu^{0.35}$. They concluded that the evolution of the core and corona of the clusters are mainly controlled by internal relaxation processes.

In Figure 12 we plot various structural parameters of the clusters, given in Tables 10 and 11, that indicate that r_c has a good correlation with $r_{\rm cn}$ and $r_{\rm cl}$. Similarly, r_c, $r_{\rm cn}$, and $r_{\rm cl}$ indicate a linear correlation with the number of stars in the core, corona, and entire cluster in the sense that a larger core and corona can accommodate a larger number of stars. The central density f_0 decreases exponentially with an increase in core radius. In Figure 13 various structural parameters from Tables 10 and 11 are plotted as a function of age that indicate that in the age range 10–1000 Myr,

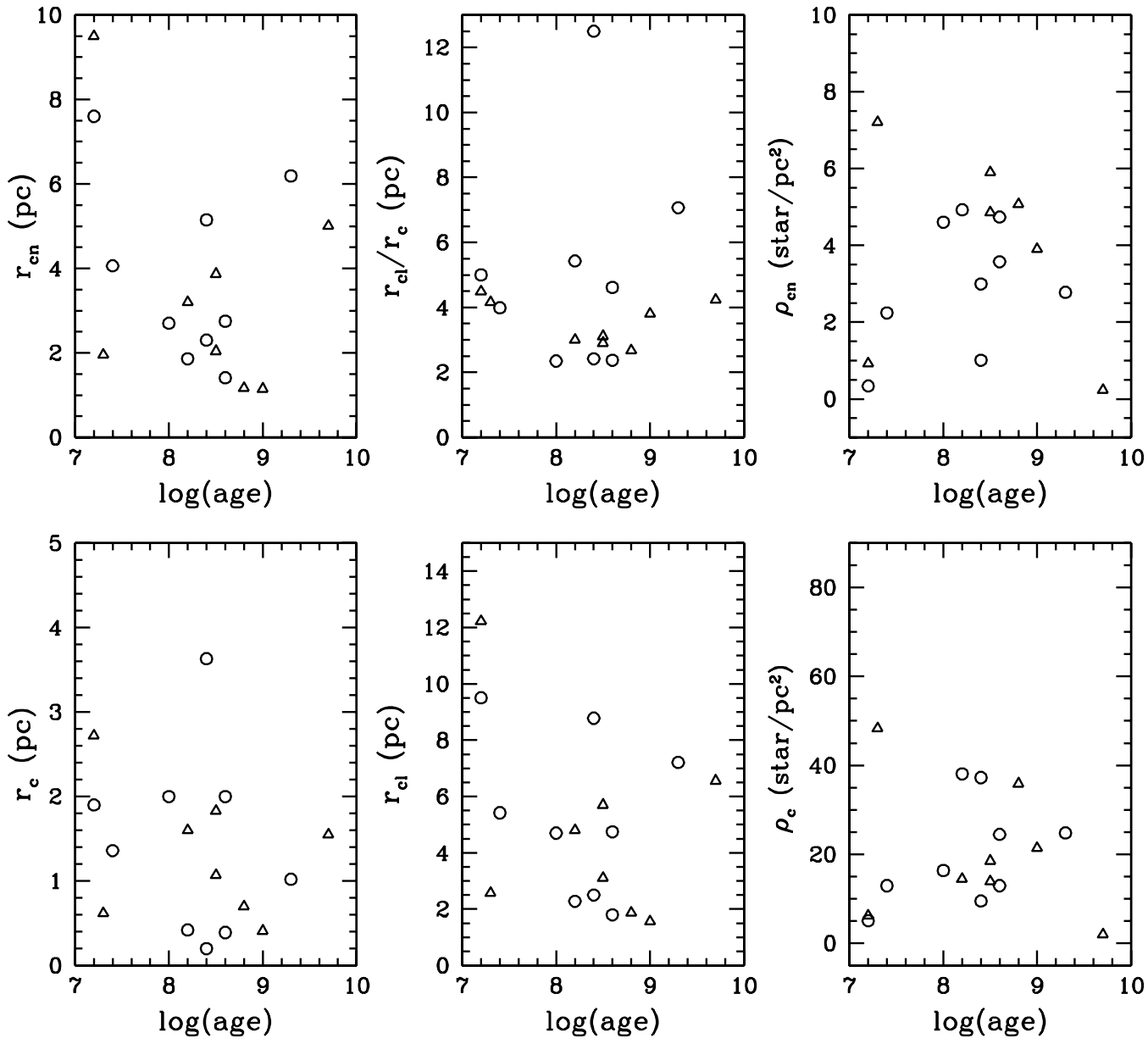

FIG. 13.—Various structural parameters of clusters as a function of age. The symbols are the same as in Fig. 11.

the core and extent of the cluster seem to shrink with age. In the case of less-massive clusters, the work of BB05 (their Fig. 7*g*) also indicates a similar correlation between age and core radius for clusters with age $\leq$1000 Myr. Because of the above correlation between age and core/corona radius, the projected surface densities in the core (ρ_c) and corona (ρ_{cn}) are higher for intermediate-age and old (100–1000 Myr) clusters as compared to younger clusters. The same trend can be noticed in Figures 7*i* and 7*l* of BB05 for less massive clusters. The concentration parameter r_{cl}/r_c is plotted as a function of age in Figure 13, indicating no trend with age. N02 have also concluded the same.

Figure 13 also indicates that the core and corona of the two oldest open clusters in the present sample (age $>10^9$ yr), namely, NGC 2420 ($r_c = 1.0$ pc, $r_{cl} = 10$ pc) and Be 20 ($r_c = 1.6$ pc, $r_{cl} = 6.6$ pc), are found to be relatively larger than the expected value of r_c ($\sim$0.5 pc) and r_{cl} ($\sim$2 pc) at age $\sim 10^9$ yr. These clusters are located at large distances (NGC 2420: $z = 844$ pc; Be 20: $z = -2700$ pc) from the Galactic plane. The large coronae of NGC 2420 and Be 20 probably indicate that these clusters may be in the process of disintegration, as suggested by C04.

The dependence of cluster sizes on galactocentric distances R_G is displayed in Figure 14. A vertical dashed line is drawn to delineate the sample of clusters with $R_G < 10$ kpc and $R_G > 10$ kpc. The figure indicates that in the range 9 kpc $< R_G <$ 10 kpc, the core, corona, and total cluster size increase with the galactocentric distance. The study of N02 also indicates a similar correlation between cluster size and R_G for $R_G > 9$ kpc.

6.2. *Summary*

This paper analyzes homogeneous wide-field CCD data of nine open clusters (ages in the range of 16 Myr to 2 Gyr) taken from the Kiso Schmidt telescope. Based on the well-defined ($U - B$, $B - V$) TCD and CMDs, we estimated the reddening toward the cluster region, distance, and age of the target clusters. The structural parameters for the target clusters were obtained using the projected radial density profile. Most of the clusters show an increase in core radius when faint cluster members are

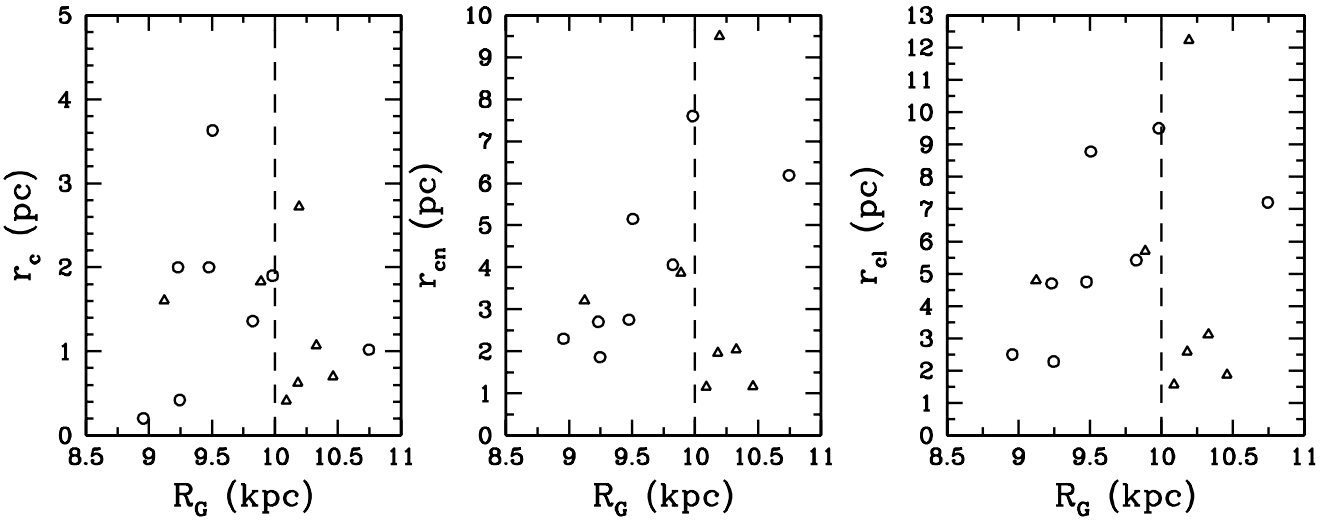

FIG. 14.—Dependence of cluster size on galactocentric distance R_G. The symbols are the same as in Fig. 11. The r_c, r_{cn}, and r_{cl} of the clusters located at 9 kpc $< R_G <$ 10 kpc show an increasing trend with increasing R_G. The vertical dashed line is drawn to delineate the samples of clusters with $R_G <$ 10 kpc and $R_G >$ 10 kpc.

included in the sample. The radial structure of all clusters can be well explained by King's (1962) empirical model. The target cluster sample indicates an elongated core for young (Be 62, log age = 7.2), as well as for intermediate-age, open clusters (NGC 2548, log age = 8.6). C04 mentioned that the clusters have a tendency toward spherical shapes away from the disk, particularly in the case of old systems, due to internal dynamical relaxation. However, we find that the relatively young cluster NGC 1960 (log age = 7.4, $z = 24$ pc) has a rather spherical core.

The present sample of clusters follows the relation $r_c/r_{cn} \propto (n_c/n_{cn})^{0.35}$, as suggested by Danilov & Seleznev (1994). It is found that the core radius and corona size/cluster radius are linearly correlated. It is also found that in the age range 10–1000 Myr, the core and corona of the cluster shrink with age. In the galactocentric distance range 9–10 kpc, the core and corona/cluster extent of the clusters increase with galactocentric distance.

We would like to thank the anonymous referee for his constructive comments. This work is partly supported by the Department of Science and Technology, India, and the Japan Society for the Promotion of Science, Japan. A. K. P. is thankful to the staff of Kiso Observatory for their help during his stay there.

REFERENCES

Amieux, G. 1988, A&AS, 76, 305
Anthony-Twarog, B. J., Kaluzny, J., Shara, M. M., & Twarog, B. A. 1990, AJ, 99, 1504
Barbaro, G., Dallaporta, N., & Fabris, G. 1969, Ap&SS, 3, 123
Barbaro, G., Dallaporta, N., & Nobili, L. 1967, Publ. Obs. Astron. Padua, 138, 1
Barkhatova, K. A., Zakharova, P. E., Malisheva, L. K., & Shashkina, L. P. 1984, Methods of Investigation in Astronomy and Geodetics (Ekaterinburg: Ural State Univ.)
Battinelli, P., Brandimarti, A., & Capuzzo-Dolcetta, R. 1994, A&AS, 104, 379
Bergond, G., Leon, S., & Guibert, J. 2001, A&A, 377, 462 (B01)
Bertelli, G., Bressan, A., Chiosi, C., Fagotto, F., & Nasi, E. 1994, A&AS, 106, 275
Bonatto, C., & Bica, E. 2005, A&A, 437, 483 (BB05)
Cannon, R. D., & Lloyd, C. 1970, MNRAS, 150, 279
Chen, W. P., Chen, C. W., & Shu, C. G. 2004, AJ, 128, 2306 (C04)
Chini, R., & Wargau, W. F. 1990, A&A, 227, 213
Claria, J. J., Piatti, A. E., & Lapasset, E. 1998, A&AS, 128, 131
Collinder, P. 1931, Ann. Obs. Lund, 2, 1
Cuffey, J. 1941, ApJ, 94, 55
Curry, C. C. 2002, ApJ, 576, 849
Danilov, V. M. 1997, Astron. Rep., 41, 163
Danilov, V. M., & Seleznev, A. F. 1994, Astron. Astrophys. Trans., 6, 85
Durgapal, A. K., & Pandey, A. K. 2001, A&A, 375, 840
Eggen, O. J. 1974, ApJ, 188, 59
———. 1975, PASP, 87, 37
———. 1981, ApJ, 247, 507
Feinstein, A., Claria, J. J., & Cabrera, A. L. 1978, A&AS, 34, 241
Forbes, D. 1981, PASP, 93, 441
Francic, S. P. 1989, AJ, 98, 888
Gutermuth, R. A., Megeath, S. T., Pipher, J. L., Williams, J. P., Allen, L. E., Myers, P. C., & Raines, S. N. 2005, ApJ, 632, 397
Harris, G. L. H., FitzGerald, M. P. V., Mehta, S., & Reed, B. C. 1993, AJ, 106, 1533
Henden, A. 2003, Henden Field Photometry (Washington: USNO), ftp://ftp.nofs.navy.mil/pub/outgoing/aah/sequence/
Hoag, A. A., Johnson, H. L., Iriarte, B., Mitchell, R. I., Hallam, K. L., & Sharpless, S. 1961, Publ. USNO, 17, 343 (H61)
Ianna, P. A., Adler, D. S., & Faudree, E. F. 1987, AJ, 93, 347
Johnson, H. L., & Morgan, W. W. 1953, ApJ, 117, 313
Kalirai, J. S., Fahlman, G. G., Richer, H. B., & Ventura, P. 2003, AJ, 126, 1402
Kaluzny, J., & Udalski, A. 1992, Acta Astron., 42, 29
Kharchenko, N. V., Piskunov, A. E., Röser, S., Schilbach, E., & Scholz, R.-D. 2005, A&A, 438, 1163 (K05)
Kholopov, P. N. 1969, Soviet Astron., 12, 625
Kim, S. L., et al. 2001, A&A, 371, 571
King, I. 1962, AJ, 67, 471
Landolt, A. 1992, AJ, 104, 340
Lee, S. H., Ann, H. B., & Kang, Y. W. 2002, in Proc. IAU 8th Asian-Pacific Regional Meeting, Vol. II, ed. S. Ikeuchi, J. Hearnshaw, & T. Hanawa (Tokyo: Astron. Soc. Japan), 273
Leonard, P. J. T. 1988, AJ, 95, 108
Lynga, G. 1984, Catalogue of Open Clusters (Strasbourg: CDS)
Lynga, G., & Palous, J. 1987, A&A, 188, 35
McClure, R. D., Forrester, W. T., & Gibson, J. 1974, ApJ, 189, 409
McClure, R. D., Newell, B., & Barnes, J. V. 1978, PASP, 90, 170
Mermilliod, J. C. 1995, in Information and On-Line Data in Astronomy, ed. D. Egret & M. A. Albrecht (Dordrecht: Kluwer), 127
Miller, G. E., & Scalo, J. M. 1979, ApJS, 41, 513
Mohan, V., & Sagar, R. 1988, Bull. Astron. Soc. India, 16, 159
Mostafa, A. A., Hassan, S. M., Aiad, A., & Ahmed, I. 1983, J. Astron. Soc. Egypt, 5, 23
Napiwotzki, R., Schönberner, D., & Weidemann, V. 1991, A&A, 243, L5
Nilakshi, Sagar, R., Pandey, A. K., & Mohan, V. 2002, A&A, 383, 153 (N02)
Nissen, P. E. 1988, A&A, 199, 146
Pandey, A. K., Bhatt, B. C., & Mahra, H. S. 1991, Mem. Soc. Astron. Italiana, 62, 927

Pandey, A. K., Mahra, H. S., & Sagar, R. 1990, AJ, 99, 617
Pandey, A. K., Nilakshi, Ogura, K., Sagar, R., & Tarusawa, K. 2001, A&A, 374, 504
Pandey, A. K., Ogura, K., & Sekiguchi, K. 2000, PASJ, 52, 847
Pandey, A. K., Upadhyay, K., Nakada, Y., & Ogura, K. 2003, A&A, 397, 191
Pandey, A. K., Upadhyay, K., Ogura, K., Sagar, R., Mohan, V., Mito, H., Bhatt, H. C., & Bhatt, B. C. 2005, MNRAS, 358, 1290
Pandey, A. K., et al. 2006, MNRAS, submitted
Pastoriza, M. G., & Ropke, U. O. 1983, AJ, 88, 1769
Pesch, P. 1961, ApJ, 134, 602
Phelps, R. L., & Janes, K. A. 1994, ApJS, 90, 31
Rieke, C. A. 1935, Harvard Coll. Obs. Circ., 397, 1
Sanner, J., Altmann, M., Brunzendorf, J., & Geffert, M. 2000, A&A, 357, 471
Sarma, M. B. K., & Walker, M. F. 1962, ApJ, 135, 11
Schmidt-Kaler, Th. 1982, in Landolt-Börnstein: Numerical Data and Functional Relationships in Science and Technology, ed. K. Schaifers, H. H. Voigt, & H. Landolt (Berlin: Springer), 19
Shapley, H. 1930, Star Clusters (New York: McGraw-Hill)
Smyth, M. J., & Nandy, K. 1962, Publ. R. Obs. Edinburgh, 3, 24
Stetson, P. B. 1987, PASP, 99, 191
———. 1992, in ASP Conf. Ser. 25, Astronomical Data Analysis Software and Systems I, ed. D. M. Warrall, C. Biemesderfer, & J. Barnes (San Francisco: ASP), 297
———. 2000, PASP, 112, 925
Trumpler, R. 1930, Lick. Obs. Bull., 14, 154
Twarog, B. A., Ashman, K. M., & Anthony-Twarog, B. J. 1997, AJ, 114, 2556
West, F. R. 1967, ApJS, 14, 384